Baranek, T., Manh, T.-P.V., Alexandre, Y., Maqbool, M.A., Cabeza, J.Z., Tomasello, E., Crozat, K., Bessou, G., Zucchini, N., Robbins, S.H., Vivier, E., Kalinke, U., Ferrier, P., Dalod, M.
Differential responses of immune cells to type i interferon contribute to host resistance to viral infection
(2012) Cell Host and Microbe, 12 (4), pp. 571-584.

Differential responses of immune cells to Type I interferon contribute to host resistance to viral infection

Thomas Baranek[1,2,3*,**], Thien-Phong Vu Manh[1,2,3*], Yannick Alexandre[1,2,3], Muhammad Ahmad Maqbool[1,2,3], Joaquin Zacarias Cabeza[1,2,3], Elena Tomasello[1,2,3], Karine Crozat[1,2,3], Gilles Bessou[1,2,3], Nicolas Zucchini[1,2,3], Scott H. Robbins[1,2,3***], Eric Vivier[1,2,3,4], Ulrich Kalinke[5], Pierre Ferrier[1,2,3], Marc Dalod[1,2,3]

[1]Centre d'Immunologie de Marseille-Luminy, UNIV UM2, Université de la Méditerranée, Parc scientifique et technologique de Luminy, 13288 Marseille, France
[2]Institut National de la Santé et de la Recherche Medicale (Inserm), UMR1104, 13288 Marseille, France
[3]Centre National de la Recherche Scientifique (CNRS), UMR7280, 13288 Marseille, France
[4]Assistance Publique – Hôpitaux de Marseille, Hôpital de la Conception, 13385 Marseille, France
[5]Institute for Experimental Infection Research, TWINCORE, Centre for Experimental and Clinical Infection Research, a joint venture between Hannover Medical School (MHH) and the Helmholtz Centre for Infection Research (HZI), Hannover, Germany

Contact
Marc Dalod, Centre d'Immunologie de Marseille-Luminy, Campus de Luminy, Case 906, F-13288 Marseille cedex 09, France; e-mail: dalod@ciml.univ-mrs.fr; phone: +33-4-91-26-94-51; fax: +33-4-91-26-94-30

Additional Footnotes:
*TB and TPVM contributed equally to this work.
**Present address: Université François Rabelais UMR 1100, Centre d'Etude des Pathologies Respiratoires, F-37032 Tours, France
***Present address: Immune Design Corporation, Seattle, USA

Running Title: **Shaping of innate antiviral response by type I IFN**

Keywords: dendritic cell subsets; natural killer cells; murine cytomegalovirus infection; type I interferons; IL-15; transcriptomic analysis

Abbreviations: BM, Bone Marrow; BMC, Bone Marrow Chimera; cDC, conventional dendritic cells; DC, dendritic cells; DEG, differentially expressed genes; FDR, False Discovery Rate; GSEA, Gene Set Enrichment Analysis; IFNAR, Type I interferon receptor; Type I IFN, Type I interferons; IL12/18SG, IL-12- or IL-18-Stimulated Genes; IL15SG, IL-15-Stimulated Genes; IPA, Ingenuity Pathway Analysis; ISG, Type I IFN-Stimulated genes; MCMV, mouse cytomegalovirus; MHC, major histocompatibility complex; NES, Normalized Enrichment Score; NI, not infected; NK, natural killer; pDC, plasmacytoid dendritic cell; polyIC, polyinosinic:polycytidylic acid; TFBS, Transcription Factor Binding Site; TLR, toll-like receptor; TSS, Transcription Start Site

Graphical abstract:

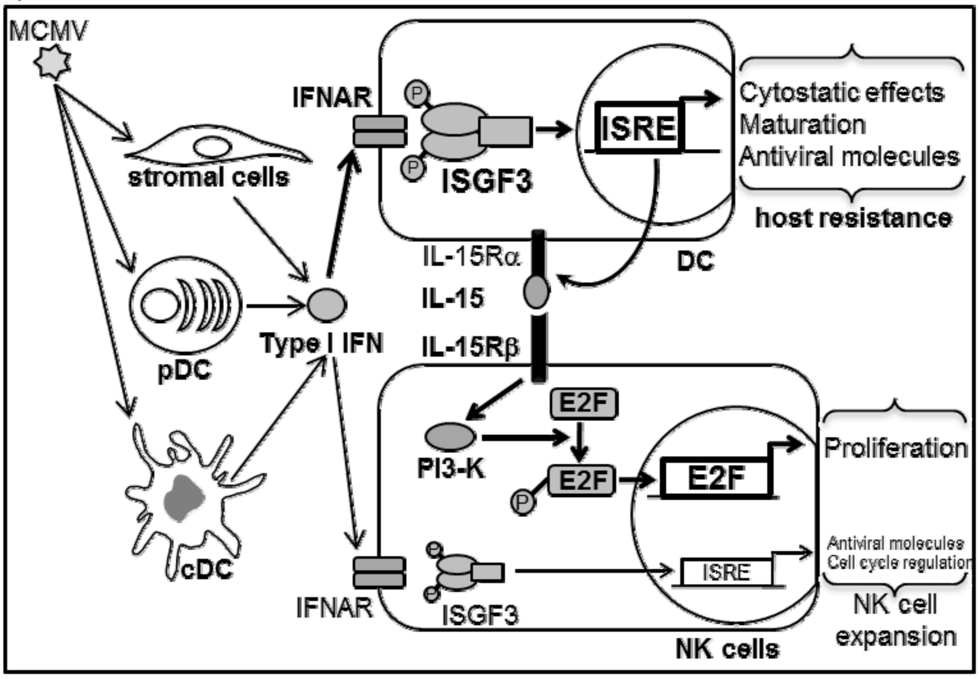

Highlights:

Type I IFN mediate different effects on DC and NK cells during MCMV infection

Type I IFN shape antiviral DC responses in a cell-intrinsic ISGF3-dependent manner

Type I IFN shape antiviral NK cell activity indirectly via an IL-15→PI3K→E2F signal

Type I IFN cell-intrinsic responses in DC but not NK cells promote host resistance

Summary

Type I interferons (IFN) are central to antiviral defense but how they orchestrate immune cell function is incompletely understood. We determined that Type I IFN produced during murine cytomegalovirus (MCMV) infection differentially affect dendritic cells (DC) and natural killer (NK) cells. Type I IFN induce cell-intrinsic responses in DC, activating anti-proliferative, antiviral and lymphocyte-activating gene networks, consistent with high activity of the transcription factor STAT1 in these cells. By comparison, NK cells exhibit lower STAT1 expression and reduced Type I IFN responsiveness. Rather, type I IFN indirectly affect NK cells by inducing IL-15, which activates the transcription factor E2F and stimulates genes promoting cell expansion. Type I IFN cell-intrinsic responses are necessary in DC but not NK cells for MCMV resistance. Thus, sensitivity to type I IFN-induced cytokines and differences in type I IFN receptor signaling program immune cells to mount distinct responses that promote viral control.

Introduction

Dendritic cells (DC) are leukocytes specialized in the processing of peptide antigens and their presentation in association with major histocompatibility complex (MHC) molecules for the activation of naïve T lymphocytes. DC are crucial for adaptive immunity against cancer and infectious agents. DC and Natural killer (NK) cells also contribute to innate immune responses early after infections. Their cross-talk promotes activation or maintenance of both partners and shaping of adaptive immunity. The instructive signals involved in the regulation of DC or NK cell functions during viral infections *in vivo* are not completely deciphered.

Mouse cytomegalovirus (MCMV) infection recapitulates key physiopathological characteristics of human cytomegalovirus infection (Krmpotic et al., 2003). It is one of the rare mouse models which allow studying the interactions between a virus and its natural host. It led to outstanding advances in the understanding of immunity to viral infections (Benedict et al., 2013; Dalod and Biron, 2013). The cytokines type I interferons (type I IFN) and IL-12 are critical for resistance to MCMV infection. Type I IFN are produced initially, around 8 hours after infection, by infected stromal cells in the spleen, and later, around day 1.5, by a particular subset of DC, plasmacytoid DC (pDC). Both cell types contribute to control viral replication. Another subset of DC, CD8α$^+$ conventional DC (cDC), promotes optimal priming of antiviral CD8 T lymphocytes. Both pDC and CD8α$^+$ cDC produce IL-12 around 1.5 days after MCMV infection. A third subset of DC, CD11b$^+$ cDC, can contribute with pDC and CD8α$^+$ cDC to NK cell activation. NK cells can be critical for virus control by recognizing and killing infected cells, upon engagement of NK cell activating receptors by viral or altered self-ligands expressed by infected cells. Several such receptor/ligand pairs have been identified in C57BL/6 mice and other resistant mouse strains (Pyzik et al., 2011). MCMV has evolved a battery of effector molecules dedicated to the inhibition of NK cell functions, leading to a lack of control by NK cells in susceptible mouse strains, and attesting to the pressure exerted by this arm of the immune system during the co-evolution between the virus and its host (Babic et al., 2011).

During MCMV infection, IL-12 promotes NK cell IFN-γ production which contributes to viral control (Nguyen et al., 2002). Type I IFN mediate direct antiviral effects against many viruses as well as a variety of immunoregulatory functions (Biron, 2001), including the induction of IL-15 and of DC maturation during MCMV infection (Dalod and Biron, 2013). Type I IFN promote NK cell entry into cell cycle, proliferation, survival and cytotoxicity (Nguyen et al., 2002). Some of these effects may be indirect, mediated by IL-15, although this is disputed (Nguyen et al., 2002; Sun et al., 2009). In other conditions, contrasting results have been published. Direct triggering of the type I IFN receptor (IFNAR) on NK cells promoted immune defense against vaccinia virus infection (Martinez et al., 2008). In response to toll-like receptor (TLR) ligand administration, NK cell activation by type I IFN occurred indirectly, through the induction of IL-15 trans-presentation by DC (Lucas et al., 2007). More generally, depending on the cell types examined, type I IFN can either promote or inhibit cell proliferation and survival (Biron, 2001). Such opposite effects might be achieved through cell type- or activation-dependent regulation of the expression of individual signaling components downstream of IFNAR (Dalod and Biron, 2013; Miyagi et al., 2007).

Here, we combined the use of functional genomics, of flow cytometry analysis of transduction molecule phosphorylation and of mutant mice, to investigate how MCMV infection modulates the gene expression program and the antiviral activity of DC subsets and NK cells, in particular the role of type I IFN.

Results

Hundreds of genes are modulated specifically in DC versus NK cells during MCMV infection

To assess the general impact of MCMV infection on splenic DC subsets and NK cells early after virus inoculation, we profiled their gene expression programs directly *ex vivo* after isolation from control animals (q_cell: quiescent cell) or infected mice (a_cell: activated cell). Two independent microarray replicates were generated for each condition. Principal component analysis (PCA) showed a close proximity of replicates (Figure 1A). Principal component (PC)1 corresponding to 'DC-ness versus NK cell-ness' represented 34% of the overall variability between microarrays. PC3, corresponding to 'DC subset-ness', and PC2, contributing to 'activation versus quiescence', accounted for a similar fraction of microarray variability, respectively 16% and 18%. Hence, belonging to a given subset and the activation status contributed equally to the shaping of the gene expression programs of DC subsets. On PC2 axis, the distance between a_DC and q_DC subsets was much longer than between a_NK and q_NK cells. In addition, a_cDC subsets were closer to one another than to their quiescent counterparts. This suggested that common and profound changes affected specifically the gene expression reprogramming of DC subsets but not NK cells during MCMV infection. To assess this, we identified the differentially expressed genes (DEG) modulated in DC subsets or NK cells upon MCMV infection, based on statistical significance and on a fold change above 2. Venn diagrams showed that 565 Probesets (representing 423 genes) were induced, and 267 ProbeSets (231 genes) were inhibited, commonly in all three DC subsets, out of which only 121 and 46 ProbeSets were modulated similarly in NK cells (Figure 1B-C). Reciprocally, 957 Probesets were induced and 775 Probesets inhibited specifically in NK cells. Hence, hundreds of genes are modulated specifically either in all DC subsets or in NK cells during MCMV infection.

Opposite regulation of genes controlling cell cycle entry in cDC and NK cells during MCMV infection

To gain insights into the functions of DC subsets and NK cells during MCMV infection and their regulation, we examined the annotations of the genes modulated in 1) all DC subsets and NK cells, 2) in all DC subsets but not in NK cells, 3) only in cDC subsets, 4) only in pDC, or 5) only in NK cells, using Ingenuity Pathway Analysis (IPA). The most significant pathways associated with the genes up-regulated in NK cells only were linked to the induction of cell proliferation (Figure 1B). The set of genes down-regulated in DC and NK cells were also enriched for annotations linked to cell proliferation or to cell death (Figure 1C). Analysis of individual gene expression profiles suggested the up-regulation of genes associated with mitosis in NK cells contrasting with their down-regulation in cDC (Figure 1D, *Ccnb2* and *Ccna2*). In contrast, the *Slfn1* and *Cdkn2b* genes involved in cell cycle entry inhibition were induced specifically in cDC (Figure 1E). Using the COXPRESdb website, we retrieved the 300 genes the most significantly co-expressed with *Ccnb2*, *Slfn1* or *Cdkn2b* based on global mining of the Gene Expression omnibus (GEO) database. We analyzed the enrichment of these 3 GeneSets in pairwise comparisons of cell subsets, by performing Gene Set Enrichment Analysis (GSEA) (Figure 1F-G and see Table S1 available online). Examples of individual enrichment plots are shown (Figure 1F). The information of many enrichment plots was synthesized as a 'dot blot', to allow visualizing the most important changes at a glance (Figure 1G). This representation showed opposite regulation of the Ccnb2 GeneSet between cDC and NK cells during MCMV infection. It was induced in a_NK cells but inhibited in a_CD8α and a_CD11b DC. While q_cDC expressed the Ccnb2 GeneSet at much higher levels than q_NK cells, the situation was reversed in a_cells. The Ccnb2 GeneSet was strongly associated with mitosis (130 genes annotated "Cell cycle", $p=1.3x10^{-113}$, including 88 genes annotated "M phase", $p=1.8x10^{-88}$). Hence, spleen cDC express a mitotic signature at steady state, reflecting their own proliferation in the spleen or their fast *in situ* renewal from actively proliferating pre-cDC (Naik et al., 2006). In contrast, spleen NK cells appear to be largely resting. During MCMV infection this picture appears completely reversed based on our gene expression analysis, which is consistent with the induction of NK cell proliferation contrasting with the attrition of cDC numbers observed in this model (Benedict et al., 2013; Dalod and Biron, 2013). Hence, MCMV infection induced an opposite regulation of genes controlling cell proliferation in cDC and NK cells.

MCMV infection selectively induces type I IFN-stimulated genes in DC and IL-15-stimulated genes in NK cells

The most significant pathways associated with the genes up-regulated in all cells or in DC subsets but not NK cells included DC maturation and the induction of antiviral defense by type I IFN (Figure 1B). Analysis of the “Interferon signaling” pathway pointed out a higher expression of *Stat2* mRNA in DC as compared to NK cells (Figure 2A). In contrast, the genes encoding the 2 IFNAR chains were not expressed to higher levels in cDC than in NK cells (Figure 2B). When examining expression of the individual 9 genes of the IPA “Interferon signaling” pathway, DC did express much higher levels of *Stat2* than NK cells. This was also the case for *Stat1* and the other type I IFN-stimulated genes (ISG) examined (Figure 2C). Hence, these analyses suggested that DC responded more strongly to type I IFN than NK cells *in vivo* during MCMV infection. To further decipher the signals driving changes in DC subset versus NK cell gene expression programs during MCMV infection, we performed GSEA analysis using large GeneSets corresponding to the known target genes of type I IFN, IL-15 and IL-12/IL-18 (Figure 2D and Table S2). The ISG GeneSet, which includes 1,452 different ProbeSets, was significantly enriched in all a_DC subsets, as compared to their quiescent counterparts and to a_NK cells (Figure 2D). In contrast, the genes stimulated by IL-15 (IL15SG GeneSet), type I IFN or IL-15 (ISG-IL15SG), or IL-12/18 (IL12/18SG) were significantly enriched in a_NK cells. Reciprocally, the genes inhibited by IL-15 were significantly repressed in a_NK cells. These results were confirmed by real-time quantitative RT-PCR for 76 genes representative of different GeneSets (Figure 2E). Hence, DC subsets harbored stronger responses to type I IFN and NK cells stronger responses to IL-15 during MCMV infection. A significant enrichment of the ISG GeneSet in a_CD8α DC as compared to a_NK cells was also observed upon *in vivo* injection of polyinosinic:polycytidylic acid (polyIC), another stimulation leading to high systemic type I IFN production but in the absence of replicative agent(see Figure S1A available online). Both upon MCMV infection and polyIC injection, many ISG were induced to higher levels in CD8α cDC than in NK cells (Figure S1B). The ISG induced in DC were associated to antiviral defense or cross-talk between DC and NK cells while the IL15SG induced in NK cells were associated to mitosis (Figure 3). Altogether, these data led us to hypothesize that type I IFN profoundly shaped antiviral DC responses *in vivo*, such that cell-intrinsic type I IFN responses of DC might be required to promote health over disease in mice infected with MCMV. In contrast, NK cell responses to MCMV infection were predicted to depend essentially on IL-15 such that cell-intrinsic type I IFN responses of NK cells might not be required to induce their proliferation, their cytotoxicity and to prevent disease.

Cell-intrinsic responses to type I IFN shape the genetic reprogramming of DC more strongly than that of NK cells

Type I IFN can directly regulate ISG in target cells through cell-autonomous IFNAR signaling. Primary ISG include several cytokines and cell surface receptors which can in turn modulate the response of neighboring cells. This causes a second, indirect, wave of ISG induction. Thus, to better understand how type I IFN shape antiviral immune responses, we examined cell-autonomous type I IFN effects on DC and NK cell responses to MCMV infection. We generated mixed bone marrow chimera (BMC) mice, by reconstituting lethally irradiated CD45.1 WT recipient animals with a 1:1 mixture of CD45.1 WT and CD45.2 IFNAR$^{-/-}$ bone marrow (BM). WT versus IFNAR$^{-/-}$ cDC and NK cells were purified from the spleen of control or infected BMC mice and the mRNA expression levels of the 76 genes analyzed in Figure 2E were measured by qRT-PCR. For the genes modulated (up- or down-regulated) during MCMV infection in WT DC or NK cells, we calculated the expression ratio between WT and IFNAR$^{-/-}$ cells from infected mice. Among the genes tested, 85% were direct targets of type I IFN in DC (Figure 4A) versus 46% in NK cells (Figure 4B). To explore more broadly cell-intrinsic type I IFN responses during MCMV infection, we performed genome wide expression profiling of WT versus IFNAR$^{-/-}$ cDC subsets and NK cells from untreated versus infected IFNAR$^{-/-}$/WT BMC mice. A higher proportion of the DEG were modulated by cell-intrinsic type I IFN signaling in DC subsets as compared to NK cells (54% of type I IFN-dependent DEG in CD8α DC, 47% in CD11b DC and

23% in NK cells, Figure 5A-C). 65 genes were found up-regulated commonly in NK cells and DC subsets. Among these genes, 31 were dependent on cell-intrinsic type I IFN responses in both DC and NK cells, but they almost all reached higher expression levels in a_DC (Figure 5D). In addition, 57 genes were induced specifically in DC subsets but not in NK cells in a manner depending on cell-intrinsic type I IFN responses (Figure 5E). Many of these genes were also induced much more strongly in CD8α cDC than in NK cells *in vivo* upon polyIC injection (*Slfn1*, *Tor1aip2, Frmd4a*, *B430306N03Rik* and *Il15* in Figure S1B and data not shown). Thus, type I IFN strongly and directly shape the genetic reprogramming of DC upon MCMV infection whereas type I IFN cell-intrinsic effects are weaker or different in NK cells.

Type I IFN responses during MCMV infection are not associated with a major induction of DC apoptosis

The most significant annotations for the IL15SG, and to a minor extent the ISG, induced specifically in NK cells were linked to cell cycle, while some of the ISG induced in DC were associated to apoptosis (Figure 3). This suggested that, in MCMV-infected animals, type I IFN might promote NK cell entry into cell cycle (Nguyen et al., 2002) and drive DC apoptosis. However, GSEA analysis showed a modest but significant enrichment not only of pro-apoptotic but also of anti-apoptotic GeneSets in a_cDC as compared to their quiescent counterparts and to a_NK cells (Figure S2A). This was confirmed by examining individual gene expression patterns (Figure S2B-C). Hence, it was impossible to hypothesize what the final impact of the infection is on cDC apoptosis. Therefore, we quantified by flow cytometry the proportion of apoptotic cells within spleen DC subsets and NK cells from infected mice (Figure S2D). The proportion of apoptotic cells, showing both caspase activity (FAM fluorescence) and plasma membrane permeability (7AAD signal), remained low during the course of infection, and was not higher in DC subsets than in NK cells. Of note, cDC showed a higher proportion of caspase^{+}7AAD^{-}, non-apoptotic, cells as compared to pDC and NK cells, consistent with a higher expression of caspase mRNA in cDC both constitutively and after infection, especially for caspase 1 and 7 (not shown), which may confer to cDC pro-inflammatory functions rather than a heightened susceptibility to apoptosis. Thus, in our experimental conditions, the strong type I IFN responses induced in DC during MCMV infection did not lead to a massive apoptosis of these cells.

Cell-intrinsic responses to type I IFN promote DC maturation and shut off replenishment of the splenic pool of immature DC from progenitors

Flow cytometry analyses confirmed that cell-intrinsic type I IFN responses induced Ly6A and Ly6C on both DC and NK cells (Figure 4C), and CCR7, CD86 and OX40 on DC (Figure 4D). A kinetic analysis of the percentages of cDC subsets within WT versus IFNAR$^{-/-}$ splenocytes in BMC mice during the course of MCMV infection showed a sharp and sustained decrease in WT cDC that was strongly attenuated for IFNAR$^{-/-}$ cDC (Figure S3A). No significant differences in the proportions of pDC or NK cells were observed between WT and IFNAR$^{-/-}$ splenocytes. MCMV infection caused a sharp decrease in the numbers of cDC progenitors in the spleen of WT mice, sustained for at least 5 days and closely paralleling the drop in the numbers of cDC (Figure S3B). The splenic pool of CD27^{+}CD11b^{-} NK cell progenitors and of mature NK cells decreased only early and transiently, starting to replenish 2 days after infection. During MCMV infection, type I IFN directly inhibited in DC, but enhanced in NK cells, the expression of genes promoting cell cycle progression (Figure 4A-B, *Mcm3* and *Rad51*). Hence, it is possible that the decrease in the expression of cell cycle genes observed in splenic DC from infected mice reflects a temporary shut-off of their replenishment from circulating and actively cycling precursors freshly emigrated from the BM, which might be the main mechanism driving DC attrition during MCMV infection rather than DC apoptosis. Thus, DC responses to MCMV are characterized by the inhibition of proliferation and the induction of maturation, both of which strongly depend on cell-intrinsic type I IFN effects.

Cell-intrinsic responses to type I IFN are not required for NK cell proliferation and acquisition of effector functions

Induction of IFN-γ, Ki67, FasL and 4-1BB protein expression was comparable between IFNAR$^{-/-}$ and WT NK cells in d1.5 MCMV-infected BMC mice (Figure 4E). While Granzyme B expression was significantly lower in IFNAR$^{-/-}$ than in WT a_NK cells from infected mice (Figure 4E), it was still strongly induced above the levels observed in uninfected animals (not shown). During the course of MCMV infection in BMC mice, the percentages of Ki67^{+} NK cells increased in tight parallel in WT and IFNAR$^{-/-}$ splenocytes. IFNAR$^{-/-}$ Ly49H^{+} NK cells expanded as efficiently as WT ones (Figure S3A). Thus, NK cell responses to MCMV infection are characterized by the induction of cell proliferation, IFN-γ production and cytotoxic activity, which do not require cell-intrinsic type I IFN effects.

Enrichment for different transcription factor binding sites between ISG and ISG-IL15SG

We investigated whether the genetic reprogramming of DC and NK cells after MCMV infection were driven by distinct transcription factors. We checked *in silico* the enrichment for known transcription factor binding sites (TFBS) in the promoter sequences of co-regulated genes. We extracted from each cytokine GeneSet the lists of genes that were found up-regulated by GSEA analyses in either a_DC or a_NK cells as compared to q_DC or q_NK cells. We retrieved 209 up-regulated in all a_DC subsets. We also retrieved 108 ISG-IL15SG, 453 IL15SG and 412 IL12/IL18SG up-regulated in a_NK cells. We used PASTAA (Roider et al., 2009) to look for significantly over-represented TFBS in these genes (Table S3). As expected, the ISG up-regulated in all a_DC subsets showed a significant enrichment for IRF7, IRF, and ISRE TFBS. In the IL12-IL18SG up-regulated in NK cells, no significant TFBS enrichment was observed. The IL15SG up-regulated in NK cells were enriched for E2F and PAX1/2 TFBS. Strikingly, the ISG-IL15SG up-regulated in NK cells were also enriched for PAX1/2 and E2F TFBS but not for IRF7 TFBS and ISRE. We also used a *de novo* motif discovery approach (MEME), to look for over-represented oligonucleotides in the regulatory sequences ([-10000;+100nt] relative to TSS) of the groups of co-regulated genes examined. The motifs identified by this approach were then compared to the matrices of known TFBS, which confirmed the enrichments for IRF7 TFBS and ISRE in the ISG up-regulated in DC, and for E2F TFBS in the IL15SG up-regulated in NK cells (data not shown). Thus, the ISG induced in DC must be transcribed consecutive to type I IFN-dependent activation of IRF7 or ISGF3 in DC and their binding to specific regulatory gene sequences. In contrast, many ISG specifically induced in NK cells are also IL-15 target genes and are enriched for the same TFBS as IL15SG and not as ISG. These analyses confirmed that most of the ISG induced in DC during MCMV infection are direct type I IFN targets, while the ISG up-regulated specifically in NK cells are in majority not direct type I IFN targets but are induced in response to the IL-15 produced by other cells in a type I IFN-dependent manner. Indeed, analyses in IFNAR$^{-/-}$/WT BM chimera confirmed that, in contrast to the induction of ISG, the induction of most of the ISG-IL15SG in NK cells during MCMV infection did not require cell-intrinsic IFNAR signaling (Figure 5 and Figure S4).

Higher expression and phosphorylation of STAT1 in DC likely contribute to their stronger responses to type I IFN

The higher response to type I IFN of DC as compared to NK cells was associated with higher levels of *Stat1* and *Stat2* mRNA both under steady state conditions and after up-regulation upon MCMV infection (Figure 2C). To confirm and extend this observation, we compared STAT1 protein expression and phosphorylation in WT versus IFNAR$^{-/-}$ DC and NK cells from uninfected versus MCMV-infected BMC mice. STAT1 protein was confirmed to be expressed at higher levels in DC as compared to NK cells at steady state conditions and even more upon MCMV infection (Figure 6A). Moreover, STAT1 phosphorylation was induced to higher levels in a_DC than in a_NK cells, in an IFNAR-dependent manner (Figure 6A). As a control, we also examined STAT4 phosphorylation which occurs in NK cells in response to both IL-12 and type I IFN stimulation (Miyagi et al., 2007). STAT4 phosphorylation was induced to high levels specifically in a_NK cells, and this was even higher in IFNAR$^{-/-}$ cells consistent with a major role of IL-12 for STAT4 activation in a_NK cells (Nguyen et al., 2002). Thus, higher expression and phosphorylation of STAT1, and likely STAT2 as well, contribute to the stronger responses to type I IFN of DC as compared to NK cells during MCMV infection.

E2F is the major transcription factor downstream of IL-15 signaling for the induction of NK cell proliferation and accumulation

Our *in silico* analyses of promoter sequences pinpointed a major involvement of E2F in NK cell responses to MCMV infection *in vivo* and to IL-15 stimulation *in vitro*. E2F is implicated in activating cell cycle genes in T lymphocytes where it can be recruited upon IL-2 stimulation (Brennan et al., 1997). However, E2F involvement in NK cell responses to viral infection or to stimulation by cytokines has not yet been reported. We next examined E2F expression and phosphorylation in NK cells during MCMV infection or IL-15 stimulation. The expression of genes encoding several members of the E2F transcription factor family was induced specifically in a_NK cells but remained unchanged or was even reduced in a_DC (Figure 6B). *In vivo,* both total and phosphorylated E2F1 were up-regulated in a_NK cells (Figure 6C). *In vitro*, IL-15-stimulated NK cells expressed high level of E2F1 and phospho-E2F1 upon IL-15 stimulation as compared to untreated or type I IFN-stimulated NK cells (Figure 6D). The induction of T lymphocyte proliferation by IL-2 depends on E2F activation by the Phosphatidylinositol 3-Kinase (PI3K), in a Stat5- and Raf/MEK-independent manner (Brennan et al., 1997). Similarly, both the up-regulation of E2F1 and its phosphorylation upon IL-15 stimulation were reduced in NK cells pretreated with LY294002, a PI3K pharmacological inhibitor (Figure 6D). ChIP-PCR experiments on primary NK cells stimulated for 24 hrs with IL-15 immediately after isolation from the spleen of untreated WT mice confirmed E2F binding to its predicted target sites in the regulatory regions of the cell cycle genes *Mcm2*, Mcm3, *Mcm7*, *Dtl*, *Kif11*, *Check1* and *Cdc25a* (Figure 6E and Table S4). Of note, the MCM2-7 helicase complex, involved in DNA replication, is selectively required for the development of mature NK cell in humans by promoting the proliferation of their immediate precursors (Gineau et al., 2012). *In vivo* neutralization of IL-15 responses in WT mice, through administration of $F(ab')_2$ anti-CD122 antibody, significantly decreased the percentages of $GzmB^+$ and $Ki67^+$ NK cells, as well as the MFI for these molecules in the positive cells, while IFN-γ induction was not affected (Figure S5). Upon this treatment, a trend towards decreased expression of E2F and pE2F in NK cells was observed (Figure 6F). Thus during MCMV infection, NK cells are instructed to proliferate, accumulate and acquire cytotoxicity by an IL-15Rβ-to-PI3K-to-E2F signaling pathway, as a secondary consequence to type I IFN induction of IL-15 in other cell types.

DC but not NK cell responsiveness to type I IFN critically promotes resistance to MCMV infection

Since DC respond to type I IFN much more strongly than NK cells, this may be important for controlling viral infections. Hence, we investigated the impact on resistance to MCMV infection of the deficiency to respond to type I IFN selectively in DC (Figure 7A). We generated two sets of mixed BMC mice, by reconstituting lethally irradiated CD45.1 WT animals with a 1:1 mixture of CD45.1 CD11c-DTR and CD45.2 IFNAR$^{-/-}$ or WT BM (IFNAR$^{-/-}$/CD11c-DTR→WT versus WT/CD11c-DTR→WT mixed BMC mice, respectively). DT treatment in IFNAR$^{-/-}$/CD11c-DTR→WT BMC mice induced the depletion of WT DC, all derived from the CD11c-DTR BM, leaving only IFNAR$^{-/-}$ DC, while all other hematopoietic cell types remained constituted of 50% WT cells and 50% IFNAR$^{-/-}$ cells (data not shown). In contrast, in WT/CD11c-DTR→WT BMC mice, 50% of the DC were depleted also but all remaining DC were WT (data not shown). Upon MCMV challenge and DT injection, 50 % (10 out of 20) of the IFNAR$^{-/-}$/CD11c-DTR→WT BMC mice died 6-8 days after infection (Figure 7A). In contrast, in the absence of DT injection, only 18% (3 out of 17) IFNAR$^{-/-}$/CD11c-DTR→WT BMC mice died (Figure 7A). None of the WT/CD11c-DTR→WT mice died. Hence, mice that were impaired for type I IFN responses specifically in DC harbored enhanced mortality to MCMV infection. This also correlated with enhanced morbidity in terms of wasting, liver damage and viral loads (Figure S6). In contrast, similar experiments performed for NK cells using NKp46-hDTR mice (Narni-Mancinelli et al., 2011) did not show any impact of loss of IFNAR responsiveness (Figure 7B and Figure S6). Collectively, these results show that DC but not NK cell ability to respond to type I IFN is crucial to promote resistance to MCMV infection.

Discussion

The goal of our study was to examine the extent and specificity of the genetic reprogramming of DC subsets and NK cells during a viral infection *in vivo*, to compare the responses between these cell types, and to investigate which signals instruct them. A major aim was to determine whether type I IFN played an important role in the global shaping of DC and NK cell responses to MCMV infection, and how.

We showed that all the three spleen-resident DC subsets, pDC, CD11b$^+$ DC and CD8α$^+$ DC, underwent profound common modifications in their gene expression programs, with the induction or the inhibition of hundreds of genes after infection. Most of these genes were not modulated to the same extent in NK cells, which selectively induced or repressed different sets of hundreds of genes.

The functional annotation of different groups of co-regulated genes in DC subsets isolated from MCMV-infected mice showed induction of gene networks associated to the detection and control of viruses, and to the cross-talk with NK cells or T lymphocytes, two functions that had been previously reported to be induced upon DC maturation *in vitro* in response to virus stimulation or IFN-β treatment (Borderia et al., 2008). DC did not undergo a marked apoptosis in the spleen of infected mice but showed a profound decrease in the expression of mitosis genes. A sustained decrease of pre-cDC recruitment into the spleen was also observed. Hence, the attrition of cDC numbers occurring early after MCMV infection may result mainly from a shutdown of pre-cDC recruitment and proliferation into the spleen. NK cells up-regulated gene networks involved in mitosis. Thus, after MCMV infection, the genetic reprogramming of DC subsets endowed them with the ability to induce both innate and adaptive immune responses via the expression of antiviral sensor and effector molecules, the production of cytokines and the acquisition of plasma membrane receptors involved in lymphocyte activation. This occurred at the expense of the renewal of the splenic pool of immature DC, which appeared dispensable for antiviral defense. In contrast, the genetic reprogramming of NK cells reflected their entry into an intense proliferation phase, which may be required to generate enough numbers of innate effector cytotoxic lymphocytes to patrol all tissues for efficient detection and killing of virus-infected cells.

We next attempted to identify some of the molecular pathways instructing the genetic reprogramming of DC subsets and NK cells during MCMV infection. Many known ISG were expressed at much higher levels in DC than in NK cells and harbored potential binding sites for the two main transcription factors involved in type I IFN signaling, IRF7 and ISGF3 (an IRF-9/STAT1/STAT2 complex). DC expressed higher levels of *Irf7* and *Stat1/2* mRNA and of total and phosphorylated STAT1 protein than NK cells. Cell-intrinsic responses to type I IFN strongly modulated the expression of many more genes in DC than in NK cells during MCMV infection. In IFNAR$^{-/-}$/WT→WT mixed BMC mice, the maturation of IFNAR$^{-/-}$ DC was severely impaired, while IFNAR$^{-/-}$ NK cells were still able to proliferate, produce IFN-γ and acquire cytotoxic capacity. Loss of the cell-intrinsic capacity of DC but not NK cells to respond to type I IFN led to a significant increase in MCMV replication, disease and death in BMC mice. Thus, type I IFN played an important cell-intrinsic role in instructing the genetic reprogramming of all spleen DC subsets but not NK cells during MCMV infection.

The relatively weak NK cell response to type I IFN during MCMV infection may seem contradictory with studies describing an important role of this pathway in response to other virus-type stimuli (Gerosa et al., 2005; Martinez et al., 2008; Zhu et al., 2008). However, type I IFN can act on target cells to modulate their functions either directly or through the production and effects of other cytokines. IL-15 is induced by type I IFN and promotes NK cell activation and proliferation in response to TLR ligands (Lucas et al., 2007). During MCMV infection, the role of IL-15 in the regulation of NK cell responses is disputed (Nguyen et al., 2002; Sun et al., 2009). Here we showed that many genes responsive to IL-15 were induced to high levels specifically in NK cells during MCMV infection and harbored binding sites for E2F transcription factors. In T lymphocytes, E2F1-3 are recruited in a PI3K-dependent manner downstream to the IL-2R signaling pathway and induce genes promoting cell proliferation (Brennan et al., 1997). Similarly, we demonstrated here that E2F is activated in NK cells by IL-15 *in vitro* in a PI3K-dependent manner, and by MCMV *in vivo* in an IL-15-

dependent manner. The genes previously reported to be inducible by both type I IFN and IL-15 were specifically expressed to higher levels in a_NK cells, were enriched for E2F but not ISGF3 or IRF7 TFBS, and did not depend on cell-intrinsic type I IFN responses in NK cells. Thus, these genes must be IL-15 dependent. They were likely reported to be induced after type I IFN stimulation due to IL-15 production under the experimental conditions used. Thus, IL-15 but not type I IFN has an important cell-intrinsic role in instructing the genetic reprogramming of NK cells during MCMV infection.

In summary, we unraveled that DC and NK cells are programmed to respond to type I IFN in a strikingly different manner during a viral infection *in vivo*. We identified the underlying molecular determinism and we showed that this phenomenon contributes to the overall orchestration of immune defenses for host resistance. Specifically, we demonstrated a strong activation of the type I IFN→IFNAR→ISGF3→ISG signaling pathway in DC contrasting with the engagement of the IL-15→IL15Rβ→PI3K→E2F→IL-15SG signaling pathway in NK cells. This study demonstrates how contrasting responses of primary cell types to type I IFN can emerge as a result of a combination of i) quantitative differences in the expression levels of components of the canonical IFNAR signaling module and ii) qualitative differences in sensitivity to secondary cytokines induced by type I IFN. This explains how during a viral infection type I IFN can exert opposite effects on cell proliferation or maintenance depending on cell types. Our findings also emphasize the necessity to set up experimental procedures to discriminate cell-intrinsic versus indirect responses to type I IFN in order to understand the complex functions of these cytokines and their regulation. More than 30 genes specifically induced in DC in a cell-intrinsic IFNAR-dependent manner were not yet described as ISG to the best of our knowledge, emphasizing the need to examine cell-type specific responses to type I IFN to better understand the variety of effects caused by these cytokines *in vivo*. It will be interesting to extend these investigations to analyze the responses to type I IFN of other cell types, as well as to determine whether and how the genes regulated by type I IFN specifically in DC subsets modulate their functions.

Experimental Procedures

Mice and *in vivo* treatments.

C57BL/6J mice were purchased from Charles River Laboratories and housed at the Centre d'Immunologie de Marseille Luminy (CIML), Marseille, France. CD11c-DTR [B6.FVB-Tg(Itgax-DTR/GFP)57Lan/J), NKp46-hDTR [$Ncr1^{tm1.1(icre)Viv}$/Gt(ROSA)$26Sor^{tm1(HBEGF)Awai}$] (Narni-Mancinelli et al., 2011) and $IFNAR^{-/-}$ [B6.129S2-$Ifnar1^{tm1Agt}$] mice, all on a C57BL/6 genetic background, were bred under specific pathogen-free conditions at the CIML. Animals were used between 6 and 12 weeks of age. Infections were initiated at day 0 by i.p. injection of 10^4 or 5 x 10^4 PFU salivary gland-extracted MCMV v70 K181 strain. *In vivo* stimulation with polyIC was performed by i.p. injection of 100 µg of a high molecular weight form of drug (Invivogen). Experiments were conducted in accordance with institutional guidelines for animal care and use. For the generation of BMC mice, C57BL/6J mice were γ-irradiated once with 1000 rad from a cesium source and reconstituted with 5 × 10^6 BM cells. Under the experimental conditions used, pDC and NK cell numbers were not affected by DTA administration in WT/CD11c-DTR and $IFNAR^{-/-}$/CD11c-DTR BMC mice (not shown). IL-15 activity was neutralized *in vivo* by blocking the IL-2/IL-15Rβ subunit. Anti-IL-2Rβ mAb clone TM-β1 and control antibody (clone LTF-2) were purchased from Bio X Cell. F(ab)' was prepared using Pierce F(ab)'2 micro preparation kit (Thermo Scientific). Mice were injected 0.5 mg of F(ab)' at 2 h before, and 18 h after, MCMV infection.

Spleen preparation and flow cytometry analysis

Mice were euthanized at indicated times post-infection to collect spleen, liver and sera. Spleen leukocyte suspensions were prepared using collagenase D (Guilliams et al., 2010), stained, and acquired on a FACSCanto II flow cytometer (BD Bioscience).

Cell sorting and mRNA preparation

Each cell type studied was sorted to over 98% purity (not shown) by flow cytometry, in independent duplicate or triplicate samples. High quality RNA was prepared using commercial kits (QIAGEN) and used for microarray or real time qRT-PCR experiments.

Microarray experiments

Microarray experiments were performed and processed as previously published (Crozat et al., 2010) and detailed in supplemental experimental procedures. Datasets have been deposited in the GEO database under reference numbers GSE21491, GSE39555 and GSE39556.

GSEA analyses.

Various sets of public expression data were used to identify genes which expression was modulated by cytokines under different experimental settings (Table S2). To statistically test whether GeneSets were enriched in specific conditions or cell types, we performed pair-wise comparisons between cell types or stimulation conditions using the gene set enrichment analysis (GSEA) method from the Massachussets Institute of Technology (www.broad.mit.edu/gsea).

Real-time PCR experiments

RNA was reverse transcribed into cDNA and analyzed by real-time PCR using the $RT^2Profiler^{TM}$PCR Array System (SABiosciences). Each array contains a panel of 96 primers set including 84 selected genes, 5 housekeeping genes and 7 RNA and PCR quality controls. Relative gene expression was calculated with the ΔΔCt method using housekeeping genes for normalization.

TFBS enrichment analysis

TFBS enrichment score was assessed with PASTAA (Roider et al., 2009) against the TRANSFAC database, using the -10,000 to 0 nt relative to promoter TSS, selecting only conserved mouse/human sequence blocks.

ChIP_PCR experiments

Viable NK cells were purified by flow cytometry in independent sorts, each using pooled spleens of 25 WT C57BL/6 mice. Each sort yielded an average of 10^7 NK cells with over 98% purity. NK cells were then stimulated 24 hours with 100 ng/ml IL-15 (Miltenyi), washed and prepared for ChIP. Chromatin preparation for ChIP as well as qPCR validation experiments were performed as described previously (Koch et al., 2011), using ChIP-validated anti-E2F1 antibodies (clones KH20 and KH95, Millipore SAS) and after optimization of the process to downscale it to 20 million cells as obtained by pooling the lysate of 2 sorts. This experiment was repeated twice independently. The oligonucleotide primers used for the qPCR analysis of ChIP-ed and input DNA samples are described in Table S4.

Titration of viral loads and ALT

Viral loads were measured by conventional plaque assay on organ homogenates or by qRT-PCR on mRNA extracted from frozen tissues. Serum mouse Alanine Aminotransferase (ALT) levels were measured using a commercial ELISA kit (Euromedex). The sensitivity of the ELISA kit is 0.76U/L.

Statistical analyses.

Unless specified, statistical analyses were done using a two-tailed Student's t-test performed with Prism 5 (GraphPad Software) or Excel. *=$p<0.05$; **=$p<0.01$; ***$p<10^{-3}$.

Acknowledgements

We thank Marc Barad, Pierre Grenot, Marie-Laure Thibult and Atika Zouine for cell sorting, Aurore Fenis for help in animal breeding, Elodie Darbo for advice on computational analyses, Violaine Alunni and Christelle Thibault-Carpentier from the Plate-forme Biopuces(Strasbourg, France) for performing the microarray experiments (www-microarrays.u-stra sbg.fr). We thank Susan Chan, Philippe Kastner, Toby Lawrence, Bernard Malissen and Emilie Narni-Mancinelli for discussions or critical reading of the paper. This work was supported by Institutional funding from CNRS and Inserm, by Grants from Agence Nationale de la Recherche (ANR) (pDCphysiology, ANR-07-MIME-018-01; EMICIF, ANR-08-MIEN-008-02 and PhyloGenDC, ANR-09-BLAN-0073-02), and by the I_2HD collaborative project developed jointly by CIML and SANOFI.

Authorship

MD directed the research. MD, TB and TPVM designed experiments. TB, TPVM, YA, MAM, JZC, ET, KC, GB, NZ, SHR and MD conducted experiments and analyzed data. TPVM and MD carried out bioinformatics analyses. EV and UK provided mice. PF supervised ChIP-PCR experiments. MD, TB and TPVM wrote the paper. YA and ET gave critical comment on the paper.

Conflict-of-interest disclosure: EV is a founder and shareholder of Innate-Pharma. The gene chips experiments using IFNAR$^{-/-}$/WT mixed BMC mice were funded by SANOFI.

References

Babic, M., Krmpotic, A., and Jonjic, S. (2011). All is fair in virus-host interactions: NK cells and cytomegalovirus. Trends Mol Med 17, 677-685.

Benedict, C.A., Crozat, K., Dalod, M., and Degli-Esposti, M.A. (2013). Host Genetic Models in Cytomegalovirus Immunology. In Cytomegaloviruses: From Molecular Pathogenesis to Intervention, M.J. Reddehase, ed. (Norfolk: Caister Academic Press), pp. xxx-yyy (in press).

Biron, C.A. (2001). Interferons alpha and beta as immune regulators--a new look. Immunity 14, 661-664.

Borderia, A.V., Hartmann, B.M., Fernandez-Sesma, A., Moran, T.M., and Sealfon, S.C. (2008). Antiviral-activated dendritic cells: a paracrine-induced response state. J Immunol 181, 6872-6881.

Brennan, P., Babbage, J.W., Burgering, B.M., Groner, B., Reif, K., and Cantrell, D.A. (1997). Phosphatidylinositol 3-kinase couples the interleukin-2 receptor to the cell cycle regulator E2F. Immunity 7, 679-689.

Crozat, K., Guiton, R., Contreras, V., Feuillet, V., Dutertre, C.A., Ventre, E., Vu Manh, T.P., Baranek, T., Storset, A.K., Marvel, J., et al. (2010). The XC chemokine receptor 1 is a conserved selective marker of mammalian cells homologous to mouse CD8alpha+ dendritic cells. J Exp Med 207, 1283-1292.

Dalod, M., and Biron, C.A. (2013). Immunoregulatory Cytokine Networks Discovered and Characterized during Murine Cytomegalovirus Infections. In Cytomegaloviruses: From Molecular Pathogenesis to Intervention, M.J. Reddehase, ed. (Norfolk: Caister Academic Press), pp. xxx-yyy (in press).

Gerosa, F., Gobbi, A., Zorzi, P., Burg, S., Briere, F., Carra, G., and Trinchieri, G. (2005). The reciprocal interaction of NK cells with plasmacytoid or myeloid dendritic cells profoundly affects innate resistance functions. J Immunol 174, 727-734.

Gineau, L., Cognet, C., Kara, N., Lach, F.P., Dunne, J., Veturi, U., Picard, C., Trouillet, C., Eidenschenk, C., Aoufouchi, S., et al. (2012). Partial MCM4 deficiency in patients with growth retardation, adrenal insufficiency, and natural killer cell deficiency. J Clin Invest 122, 821-832.

Guilliams, M., Crozat, K., Henri, S., Tamoutounour, S., Grenot, P., Devilard, E., de Bovis, B., Alexopoulou, L., Dalod, M., and Malissen, B. (2010). Skin-draining lymph nodes contain dermis-derived CD103(-) dendritic cells that constitutively produce retinoic acid and induce Foxp3(+) regulatory T cells. Blood 115, 1958-1968.

Koch, F., Fenouil, R., Gut, M., Cauchy, P., Albert, T.K., Zacarias-Cabeza, J., Spicuglia, S., de la Chapelle, A.L., Heidemann, M., Hintermair, C., et al. (2011). Transcription initiation platforms and GTF recruitment at tissue-specific enhancers and promoters. Nat Struct Mol Biol 18, 956-963.

Krmpotic, A., Bubic, I., Polic, B., Lucin, P., and Jonjic, S. (2003). Pathogenesis of murine cytomegalovirus infection. Microbes Infect 5, 1263-1277.

Lucas, M., Schachterle, W., Oberle, K., Aichele, P., and Diefenbach, A. (2007). Dendritic cells prime natural killer cells by trans-presenting interleukin 15. Immunity 26, 503-517.

Martinez, J., Huang, X., and Yang, Y. (2008). Direct action of type I IFN on NK cells is required for their activation in response to vaccinia viral infection in vivo. J Immunol 180, 1592-1597.

Miyagi, T., Gil, M.P., Wang, X., Louten, J., Chu, W.M., and Biron, C.A. (2007). High basal STAT4 balanced by STAT1 induction to control type 1 interferon effects in natural killer cells. J Exp Med 204, 2383-2396.

Naik, S.H., Metcalf, D., van Nieuwenhuijze, A., Wicks, I., Wu, L., O'Keeffe, M., and Shortman, K. (2006). Intrasplenic steady-state dendritic cell precursors that are distinct from monocytes. Nat Immunol 7, 663-671.

Narni-Mancinelli, E., Chaix, J., Fenis, A., Kerdiles, Y.M., Yessaad, N., Reynders, A., Gregoire, C., Luche, H., Ugolini, S., Tomasello, E., et al. (2011). Fate mapping analysis of lymphoid cells expressing the NKp46 cell surface receptor. Proc Natl Acad Sci U S A 108, 18324-18329.

Nguyen, K.B., Salazar-Mather, T.P., Dalod, M.Y., Van Deusen, J.B., Wei, X.Q., Liew, F.Y., Caligiuri, M.A., Durbin, J.E., and Biron, C.A. (2002). Coordinated and distinct roles for IFN-alpha beta, IL-12, and IL-15 regulation of NK cell responses to viral infection. J Immunol 169, 4279-4287.

Pyzik, M., Charbonneau, B., Gendron-Pontbriand, E.M., Babic, M., Krmpotic, A., Jonjic, S., and Vidal, S.M. (2011). Distinct MHC class I-dependent NK cell-activating receptors control cytomegalovirus infection in different mouse strains. J Exp Med 208, 1105-1117.

Roider, H.G., Manke, T., O'Keeffe, S., Vingron, M., and Haas, S.A. (2009). PASTAA: identifying transcription factors associated with sets of co-regulated genes. Bioinformatics 25, 435-442.

Sun, J.C., Ma, A., and Lanier, L.L. (2009). Cutting edge: IL-15-independent NK cell response to mouse cytomegalovirus infection. J Immunol 183, 2911-2914.

Zhu, J., Huang, X., and Yang, Y. (2008). A critical role for type I IFN-dependent NK cell activation in innate immune elimination of adenoviral vectors in vivo. Mol Ther 16, 1300-1307.

Figure legends

Figure 1. Spleen DC subsets undergo a profound common genetic reprogramming during MCMV infection. Genome-wide expression analysis was performed on quiescent (q) versus activated (a) immune cells isolated from the spleen of untreated versus d1.5 MCMV-infected C57BL/6 mice. **(A)** Principal component analysis. **(B-C)** Venn diagrams represent the number of ProbeSets up-regulated **(B)** or down-regulated **(C)** >2-fold in cDC, pDC or NK cells from MCMV-infected mice as compared to untreated animals. Heatmaps represent selected functions and pathways found enriched by Ingenuity Pathway Analysis (IPA) for the sets of genes depicted in Venn diagrams. The color scale indicates the significance of the enrichment. **D-E**) Expression profiles of pro-proliferative (**D**) or anti-proliferative (**E**) genes. Data are represented as relative expression levels normalized to maximal expression across cell types (Y-axis). Data are shown as mean±SD for independent duplicates. **F-G**) Gene Set Enrichment analyses (GSEA) of the genes co-regulated with *Ccnb2*, *Slfn1* or *Cdkn2b* according to COXPRESdb. **F)** Examples of GSEA results for selected pairwise comparison between cell types. Graphical output is a bar code. Each bar corresponds to the projection of one ProbeSet of the GeneSets on the orange-to-green gradient representing all the Probesets from the gene chip ranked from high expression in population A to high expression in population B. The more the GeneSet is differentially expressed between populations, the more the bar code is shifted to one extremity. This is measured by 2 parameters. The normalized enrichment score (NES) represents the number and differential expression intensity of the genes enriched. The NES is positive if the GeneSet is enriched in the cell subset on the left (orange) and negative if it is enriched in the cell subset on the right (green). The false discovery rate (FDR) statistical value (q) represents the likelihood that the enrichment of the GeneSet represents a false positive finding (e.g. if q=0.25, a similar enrichment is found in 25% of the random GeneSets used as controls). The absolute NES values vary between ~1 and ~5. The enrichment is considered significant for absolute NES values >1 with an associated q-value <0.25. The information for each bar code can be summarized as a dot, the bigger and darker as the enrichment was stronger and more significant, in a color matching that of the cell subset in which

the GeneSet was enriched. **G)** Comprehensive GSEA show opposite regulation of the Ccnb2 GeneSet in cDC and NK cells during MCMV infection. NI=not infected. See also Table S1.

Figure 2. Bioinformatics analysis unravels contrasting roles of innate cytokine for the genetic reprogramming of DC subsets and NK cells during MCMV infection. (A) Scheme of the type I IFN signaling pathway extracted from IPA. Genes induced >2-fold in all DC subsets but not in NK cells are in red. **(B-C)** Expression profiles (mean±SD) of the type I IFN receptor chain genes (**B**) and of the IPA type I IFN signaling pathway genes (**C**). **(D)** GSEA of cytokine responding genes in DC subsets and NK cells. GeneSets corresponding to the genes stimulated or inhibited by type I IFN, IL-15 or IL12 and IL-18 were defined based on public microarray datasets. Pair-wise comparisons were performed to assess enrichment of these GeneSets between ❶ activated cell subsets from d1.5 MCMV-infected mice versus their quiescent counterparts from untreated control animals; ❷ a_DC subsets versus a_NK cells; and ❸ a_DC subsets compared to one another. **(E)** Gene expression levels in highly purified cDC and NK cells from uninfected or MCMV-infected animals as measured by qRT-PCR. Data are represented as relative expression levels normalized to maximal expression across all cell types (X-axis). Results shown are from one experiment representative of 2. See also Table S2 and Figure S1

Figure 3. Bioinformatics analysis of cytokine- and target cell-dependent effects of MCMV infection on biological processes. Heatmap representing selected functions and pathways found enriched in IPA performed on cytokine responding genes regulated in DC subsets or in NK cells during MCMV infection. See also Figure S2 and Table S3

Figure 4. Cell-intrinsic responses to type I IFN strongly shape DC but not NK cell genetic reprogramming during MCMV infection. IFNAR$^{-/-}$/WT→WT mixed BMC mice were infected or not for 1.5 days with $5x10^4$ pfu MCMV. WT versus IFNAR$^{-/-}$ DC **(A)** as well as WT versus IFNAR$^{-/-}$ NK cells **(B)** were sorted and transcript expressions were analyzed by qRT-PCR. Data represent mRNA expression

ratio (WT cells/IFNAR$^{-/-}$ cells). Data are shown only for the genes found modulated at least 2-fold in DC **(A)** or NK cells **(B)** from infected animals as compared to control mice. Green bars represent genes with a WT/IFNAR$^{-/-}$ fold change >2. Bold genes represent genes modulated in both DC and NK cells. **(C-D-E)** Splenocytes from d1.5 MCMV-infected mixed BMC mice were stained with the indicated antibodies and analyzed by flow cytometry. Proteins expressed in both DC and NK cells are represented in **(C)**, proteins expressed only in DC in **(D)** and only in NK cells in **(E)**. Results are shown as mean fluorescence intensity (MFI) ratio (WT cells /IFNAR$^{-/-}$ cells). Data are represented as mean±SEM for two (A-B) or three (C-E) independent experiments with each time ≥3 mice per group. See also Figure S3

Figure 5. Genome wide analysis of cell-intrinsic responses to type I IFN in DC subsets and NK cells from d1.5 MCMV infected IFNAR$^{-/-}$/WT BMC mice. IFNAR$^{-/-}$/WT→WT BMC mice were infected or not with MCMV. 36 hours after, splenocytes were isolated, WT versus IFNAR$^{-/-}$ NK cells, CD8α DCs and CD11b DCs purified by flow cytometry sorting and total RNA extracted for analysis on gene chips. **(A)** Venn diagram showing the overlaps between the lists of genes induced in WT cDC subsets or in NK cells from infected BMC mice as compared to uninfected animals. **(B)** Venn diagram showing the overlaps between the lists of genes induced in a cell-intrinsic IFNAR-dependent manner in cDC subsets or in NK cells. **(C)** Absolute numbers of genes induced in cDC subsets or in NK cells in an IFNAR-dependent or independent manner. **(D)** Expression profiles of the genes induced in all three cell subsets in an IFNAR-dependent manner. The heatmap was generated by regrouping genes with similar patterns of expression using the complete hierarchical clustering function of the Cluster software. For each gene, lower expression is shown in blue and higher expression in yellow. To allow better cross-comparisons of the expression patterns between genes and between two independent series of experiments, the data for each series were normalized for each gene to a mean equal to 0 and to a variance equal to 1. **(E)** Expression profiles of the genes induced specifically in cDC in an IFNAR-dependent manner. See also Figure S4.

Figure 6. Distinct transcription factors drive the genetic reprogramming of DC subsets versus NK cells in MCMV-infected mice. (A) IFNAR$^{-/-}$/WT→WT mixed BMC mice were infected or not with 5x10^{4} pfu MCMV. Intracellular expression of total STAT1, total STAT4, phospho-STAT1 and phospho-STAT4 was analyzed by flow cytometry at day 1.5 after infection. Data are from 2 independent experiments pooled together (mean±SEM, n=7). **(B)** Expression profiles (mean±SD) of the genes encoding the IL-2 receptor β chain and the E2F transcription factors. **(C)** WT mice were infected or not with 5x10^{4} pfu MCMV. Intracellular expression of total-E2F1 and phospho-E2F1 was analyzed by flow cytometry at day 1.5 after infection. Data are from 2 independent experiments pooled together (mean±SEM, n=7). **(D)** Highly purified (>95%) NK cells from WT mice were stimulated overnight *in vitro* with recombinant IFN-α (1000U/mL), IL-15 (100 ng/mL) and LY294002 (50 μM), stained with antibodies against total E2F1 or phosphorylated E2F1 and analyzed by flow cytometry. Data are representative of 2 independent experiments. **(E)** Highly purified (>98%) NK cells from WT mice were stimulated 24 hrs *in vitro* with recombinant IL-15 (100 ng/mL) and processed for ChIP using an anti-E2F1 antibody. The immunoprecipitated chromatin was examined by qRT-PCR for enrichment of target E2F1 sequences for selected IL15SG. The results are shown as Log_2 fold increase of target sequences in immunoprecipitated chromatin as compared to total input DNA. Data are representative as mean±SD for 2 independent experiments for *Mcm2*, *Mcm7*, *Dtl* and *Kif11*. **(F)** Impact of *in vivo* neutralization of IL-15 responses on the expression of phospho-E2F and E2F in NK cells from MCMV-infected mice. WT mice were treated with F(ab')$_2$ anti-CD122 or control antibody and infected with MCMV. Spleens were harvested at 1.5 days after infection and the levels of phospho-E2F and E2F were measured in NK cells by flow cytometry. Results are from one experiment representative of 2 and show MFI fold increase in NK cells (MCMV-infected animals/uninfected controls). See also Figure S5 and Table S4.

Figure 7. DC but not NK cell ability to respond to type I IFN promotes resistance to MCMV infection. IFNAR$^{-/-}$/CD11c-DTR→WT and WT/CD11c-DTR→WT mixed BMC mice **(A)** or IFNAR$^{-/-}$

/NKp46-DTR→WT and WT/NKp46-DTR→WT mixed BMC mice **(B)** were treated or not with 100ng of DT 24h before and 24h after infection with 10^4 pfu MCMV. Survival is shown for 3 independent experiments pooled together for A and one experiment for B. Statistical analysis was performed using the non-parametric Mann-Whitney test (***=p<0.001). Surviving mice were kept until day 21 post-infection. None died after day 10. See also Figure S6.

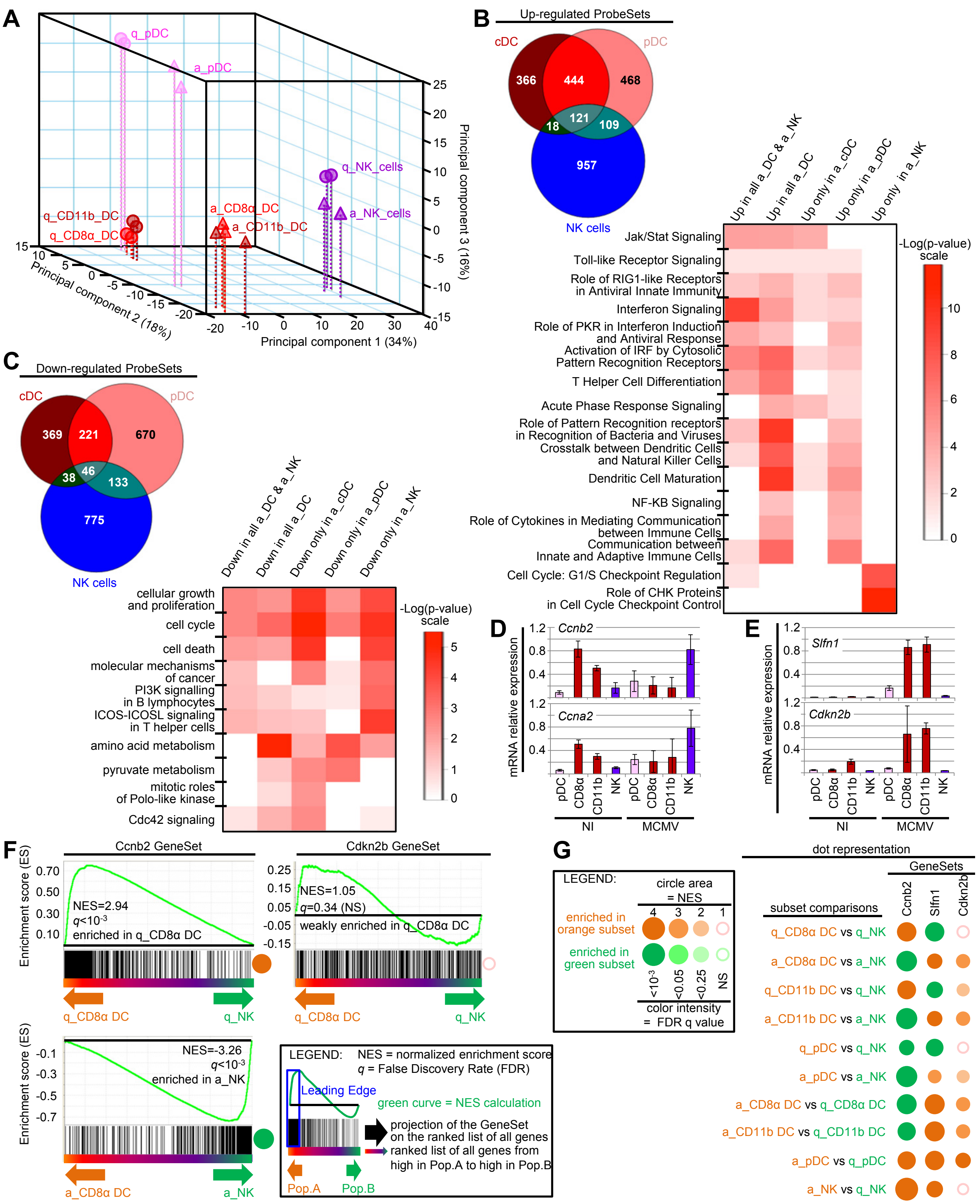
A
q_pDC
a_pDC
q_NK_cells
a_NK_cells
q_CD11b_DC
q_CD8α_DC
a_CD8α_DC
a_CD11b_DC
Principal component 1 (34%)
Principal component 2 (18%)
Principal component 3 (16%)
B
Up-regulated ProbeSets
cDC
pDC
NK cells
366
444
468
121
18
109
957
Up in all a_DC & a_NK
Up in all a_DC
Up only in a_cDC
Up only in a_pDC
Up only in a_NK
Jak/Stat Signaling
Toll-like Receptor Signaling
Role of RIG1-like Receptors in Antiviral Innate Immunity
Interferon Signaling
Role of PKR in Interferon Induction and Antiviral Response
Activation of IRF by Cytosolic Pattern Recognition Receptors
T Helper Cell Differentiation
Acute Phase Response Signaling
Role of Pattern Recognition receptors in Recognition of Bacteria and Viruses
Crosstalk between Dendritic Cells and Natural Killer Cells
Dendritic Cell Maturation
NF-KB Signaling
Role of Cytokines in Mediating Communication between Immune Cells
Communication between Innate and Adaptive Immune Cells
Cell Cycle: G1/S Checkpoint Regulation
Role of CHK Proteins in Cell Cycle Checkpoint Control
-Log(p-value) scale
C
Down-regulated ProbeSets
cDC
pDC
NK cells
369
221
670
46
38
133
775
Down in all a_DC & a_NK
Down in all a_DC
Down only in a_cDC
Down only in a_pDC
Down only in a_NK
cellular growth and proliferation
cell cycle
cell death
molecular mechanisms of cancer
PI3K signalling in B lymphocytes
ICOS-ICOSL signaling in T helper cells
amino acid metabolism
pyruvate metabolism
mitotic roles of Polo-like kinase
Cdc42 signaling
-Log(p-value) scale
D
mRNA relative expression
Ccnb2
Ccna2
pDC
CD8α
CD11b
NK
NI
MCMV
E
mRNA relative expression
Slfn1
Cdkn2b
NI
MCMV
F
Ccnb2 GeneSet
Enrichment score (ES)
NES=2.94
q<10-3
enriched in q_CD8α DC
q_CD8α DC
q_NK
Cdkn2b GeneSet
NES=1.05
q=0.34 (NS)
weakly enriched in q_CD8α DC
NES=-3.26
q<10-3
enriched in a_NK
a_CD8α DC
a_NK
LEGEND: NES = normalized enrichment score
q = False Discovery Rate (FDR)
Leading Edge
green curve = NES calculation
projection of the GeneSet on the ranked list of all genes
ranked list of all genes from high in Pop.A to high in Pop.B
Pop.A
Pop.B
G
LEGEND:
circle area = NES
enriched in orange subset
enriched in green subset
color intensity = FDR q value
dot representation
GeneSets
subset comparisons
Ccnb2
Slfn1
Cdkn2b
q_CD8α DC vs q_NK
a_CD8α DC vs a_NK
q_CD11b DC vs q_NK
a_CD11b DC vs a_NK
q_pDC vs q_NK
a_pDC vs a_NK
a_CD8α DC vs q_CD8α DC
a_CD11b DC vs q_CD11b DC
a_pDC vs q_pDC
a_NK vs q_NK

Figure 1

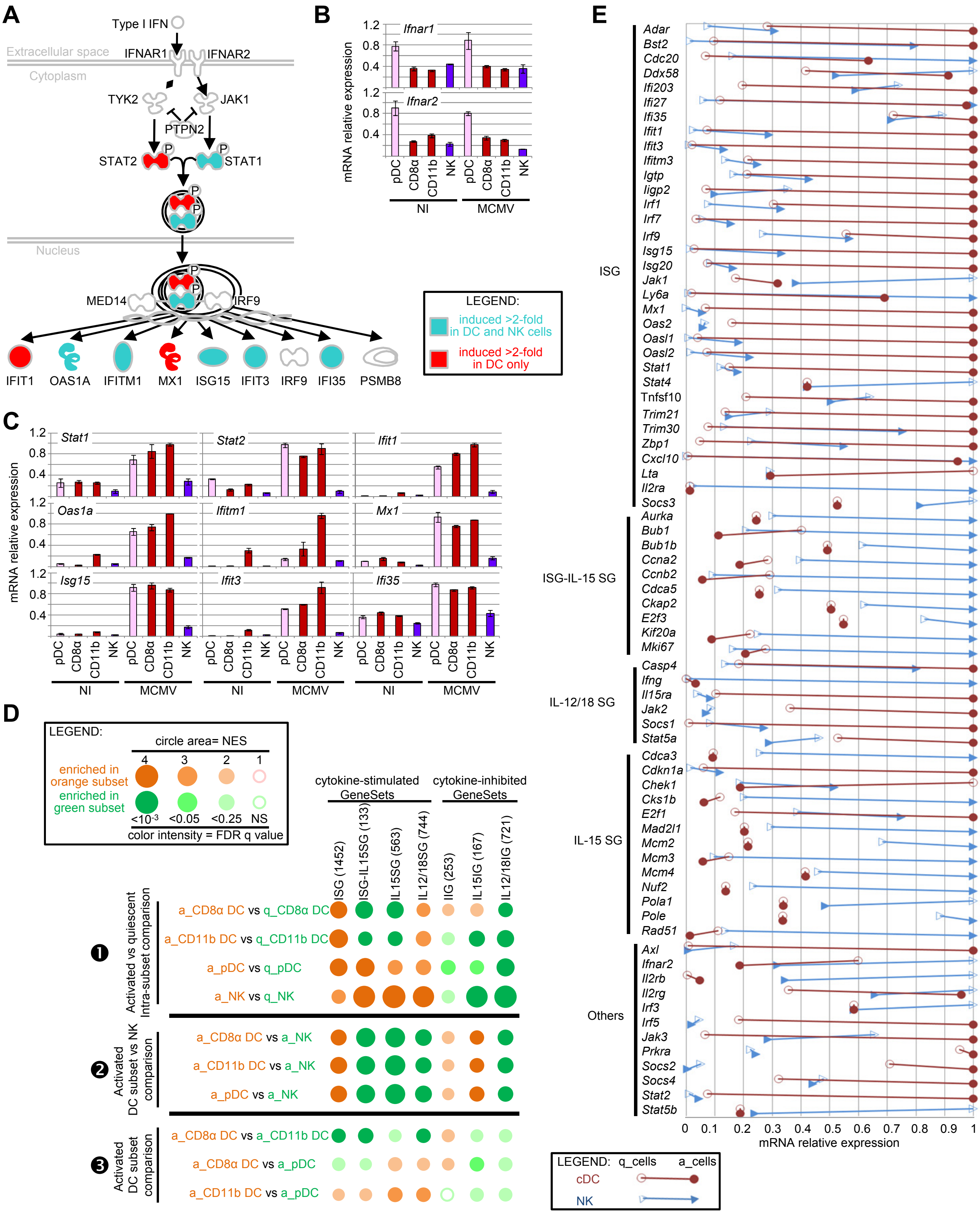
A
Type I IFN
Extracellular space
IFNAR1
IFNAR2
Cytoplasm
TYK2
JAK1
PTPN2
STAT2
STAT1
Nucleus
MED14
IRF9
IFIT1
OAS1A
IFITM1
MX1
ISG15
IFIT3
IRF9
IFI35
PSMB8
LEGEND:
induced >2-fold in DC and NK cells
induced >2-fold in DC only
B
mRNA relative expression
Ifnar1
Ifnar2
pDC
CD8α
CD11b
NK
NI
MCMV
C
Stat1
Stat2
Ifit1
Oas1a
Ifitm1
Mx1
Isg15
Ifit3
Ifi35
D
LEGEND:
circle area= NES
enriched in orange subset
enriched in green subset
color intensity = FDR q value
cytokine-stimulated GeneSets
cytokine-inhibited GeneSets
ISG (1452)
ISG-IL15SG (133)
IL15SG (563)
IL12/18SG (744)
IIG (253)
IL15IG (167)
IL12/18IG (721)
Activated vs quiescent intra-subset comparison
a_CD8α DC vs q_CD8α DC
a_CD11b DC vs q_CD11b DC
a_pDC vs q_pDC
a_NK vs q_NK
Activated DC subset vs NK comparison
a_CD8α DC vs a_NK
a_CD11b DC vs a_NK
a_pDC vs a_NK
Activated DC subset comparison
a_CD8α DC vs a_CD11b DC
a_CD8α DC vs a_pDC
a_CD11b DC vs a_pDC
E
ISG
Adar
Bst2
Cdc20
Ddx58
Ifi203
Ifi27
Ifi35
Ifit1
Ifit3
Ifitm3
Igtp
Iigp2
Irf1
Irf7
Irf9
Isg15
Isg20
Jak1
Ly6a
Mx1
Oas2
Oasl1
Oasl2
Stat1
Stat4
Tnfsf10
Trim21
Trim30
Zbp1
Cxcl10
Lta
Il2ra
Socs3
ISG-IL-15 SG
Aurka
Bub1
Bub1b
Ccna2
Ccnb2
Cdca5
Ckap2
E2f3
Kif20a
Mki67
IL-12/18 SG
Casp4
Ifng
Il15ra
Jak2
Socs1
Stat5a
IL-15 SG
Cdca3
Cdkn1a
Chek1
Cks1b
E2f1
Mad2l1
Mcm2
Mcm3
Mcm4
Nuf2
Pola1
Pole
Rad51
Others
Axl
Ifnar2
Il2rb
Il2rg
Irf3
Irf5
Jak3
Prkra
Socs2
Socs4
Stat2
Stat5b
mRNA relative expression
LEGEND: q_cells a_cells
cDC
NK

Figure 2


IL15SG up in a_NK
ISG-IL15SG up in a_NK
IL12/18SG up in a_NK
ISG up in a_CD8α DC
ISG up in a_CD11b DC
ISG up in a_pDC
ISG up in a_NK
ISG up in all a_DC & a_NK
ISG up in a_cDC
ISG up in_all a_DC not a_NK
Retinoic Acid Mediated Apoptosis Signaling
Role of PKR in Interferon Induction and Antiviral Response
Role of Pattern Recognition Receptors in Recognition of Bacteria and Viruses
Crosstalk between Dendritic Cells and Natural Killer Cells
Role of RIG1-like Receptors in Antiviral Innate Immunity
Activation of IRF by Cytosolic Pattern Recognition Receptors
Replication of cytomegalovirus
Death Receptor Signaling
Apoptosis Signaling
Antiviral response
Hematological System Development and Function
Cell Death
Role of JAK1, JAK2 and TYK2 in Interferon Signaling
RNA Post-Transcriptional Modification
Aminoacyl-tRNA Biosynthesis
Role of CHK Proteins in Cell Cycle Checkpoint Control
Cell Cycle: G1/S Checkpoint Regulation
Mitotic Roles of Polo-Like Kinase
Cell Cycle: G2/M DNA Damage Checkpoint Regulation
Cyclins and Cell Cycle Regulation
DNA Replication, Recombination, and Repair
Cell Cycle
-Log(p-value) scale
0
5
10
15
20
25
30

Figure 3

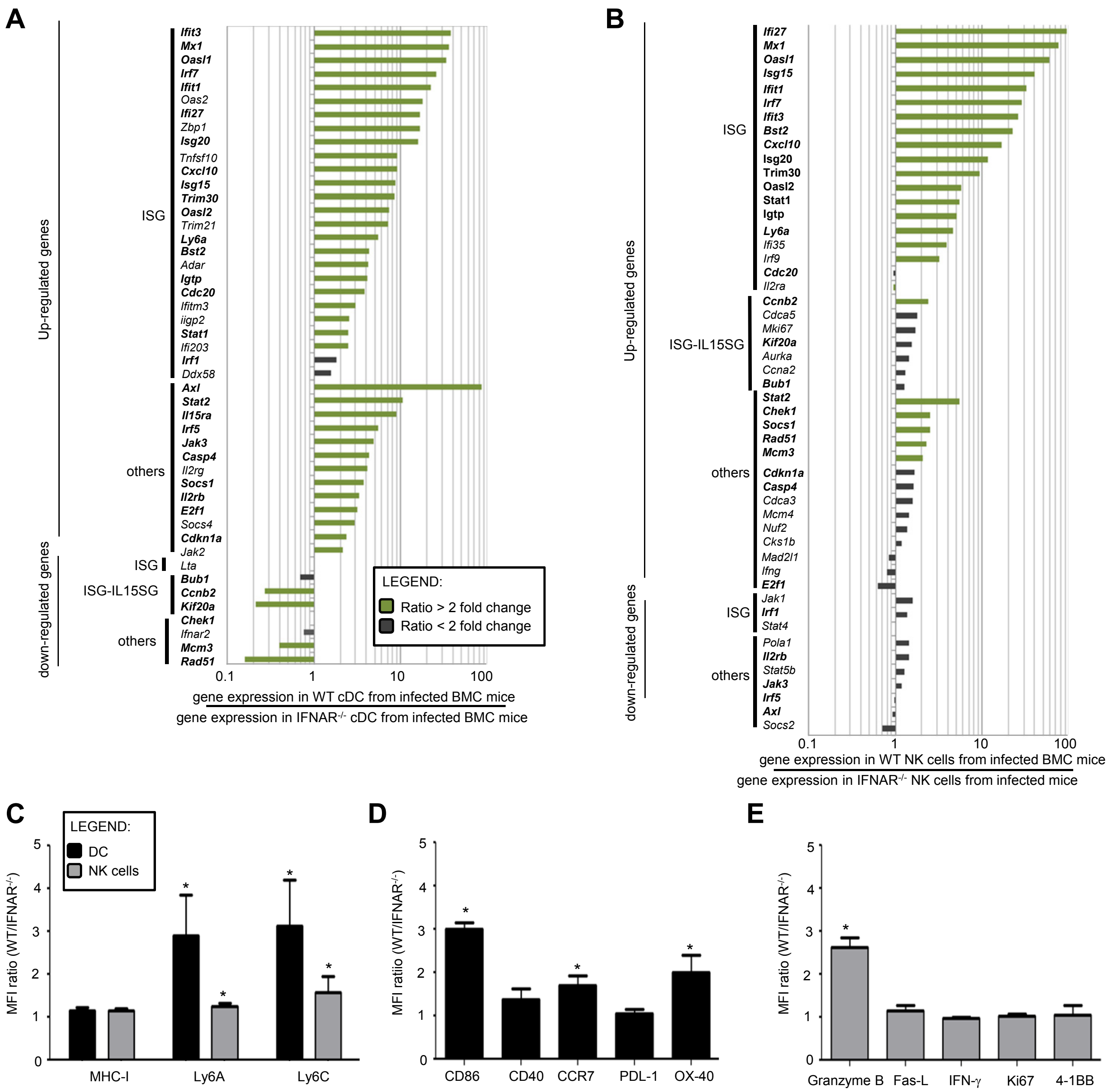
A
B
C
D
E
Up-regulated genes
down-regulated genes
ISG
ISG-IL15SG
others
LEGEND:
Ratio > 2 fold change
Ratio < 2 fold change
gene expression in WT cDC from infected BMC mice
gene expression in IFNAR-/- cDC from infected BMC mice
gene expression in WT NK cells from infected BMC mice
gene expression in IFNAR-/- NK cells from infected mice
DC
NK cells
MFI ratio (WT/IFNAR-/-)
MHC-I
Ly6A
Ly6C
CD86
CD40
CCR7
PDL-1
OX-40
Granzyme B
Fas-L
IFN-γ
Ki67
4-1BB

Figure 4

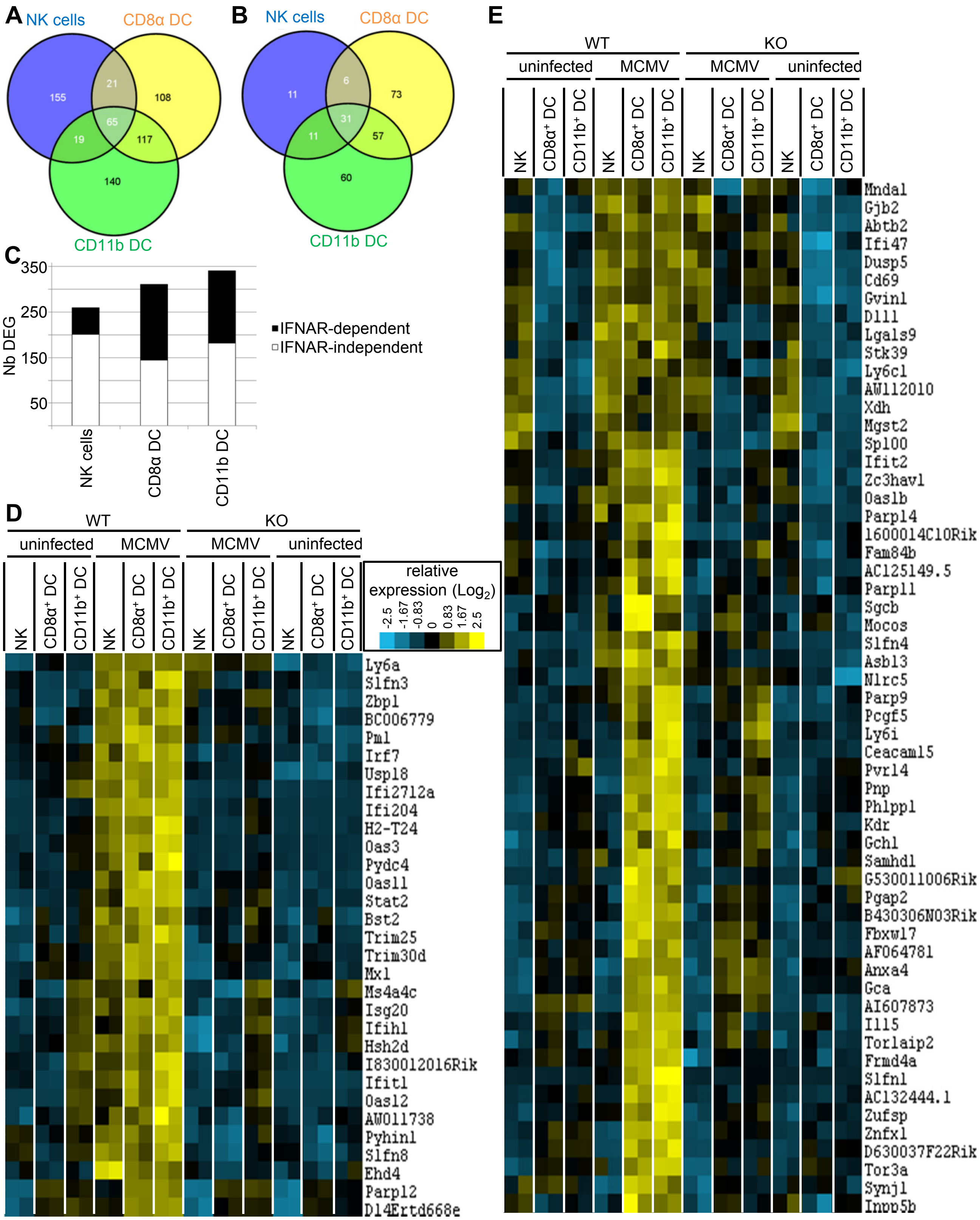
A
NK cells
CD8α DC
CD11b DC
155
21
108
65
19
117
140
B
NK cells
CD8α DC
CD11b DC
11
6
73
31
11
57
60
C
Nb DEG
350
250
150
50
NK cells
CD8α DC
CD11b DC
IFNAR-dependent
IFNAR-independent
D
WT
KO
uninfected
MCMV
MCMV
uninfected
NK
CD8α+ DC
CD11b+ DC
relative expression (Log2)
-2.5
-1.67
-0.83
0
0.83
1.67
2.5
Ly6a
Slfn3
Zbp1
BC006779
Pml
Irf7
Usp18
Ifi2712a
Ifi204
H2-T24
Oas3
Pydc4
Oasl1
Stat2
Bst2
Trim25
Trim30d
Mx1
Ms4a4c
Isg20
Ifih1
Hsh2d
I830012O16Rik
Ifit1
Oasl2
AW011738
Pyhin1
Slfn8
Ehd4
Parp12
D14Ertd668e
E
WT
KO
uninfected
MCMV
MCMV
uninfected
NK
CD8α+ DC
CD11b+ DC
Mndal
Gjb2
Abtb2
Ifi47
Dusp5
Cd69
Gvin1
Dll1
Lgals9
Stk39
Ly6c1
AW112010
Xdh
Mgst2
Sp100
Ifit2
Zc3hav1
Oas1b
Parp14
1600014C10Rik
Fam84b
AC125149.5
Parp11
Sgcb
Mocos
Slfn4
Asb13
Nlrc5
Parp9
Pcgf5
Ly6i
Ceacam15
Pvrl4
Pnp
Phlpp1
Kdr
Gch1
Samhd1
G530011O06Rik
Pgap2
B430306N03Rik
Fbxw17
AF064781
Anxa4
Gca
AI607873
Il15
Torlaip2
Frmd4a
Slfn1
AC132444.1
Zufsp
Znfx1
D630037F22Rik
Tor3a
Synj1
Inpp5b

Figure 5

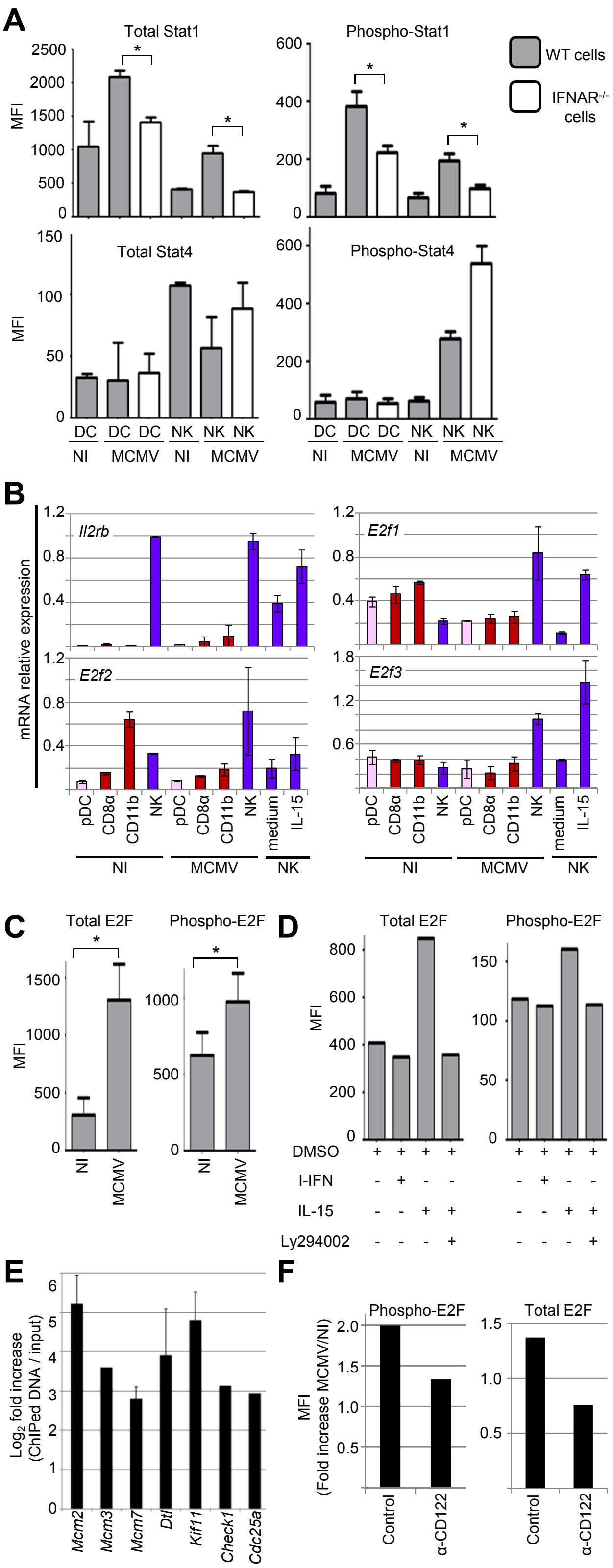
A
Total Stat1
Phospho-Stat1
WT cells
IFNAR-/- cells
MFI
Total Stat4
Phospho-Stat4
DC DC DC NK NK NK
NI MCMV NI MCMV
B
mRNA relative expression
Il2rb
E2f1
E2f2
E2f3
pDC CD8α CD11b NK pDC CD8α CD11b NK medium IL-15
NI MCMV NK
C
Total E2F
Phospho-E2F
NI MCMV
D
Total E2F
Phospho-E2F
DMSO
I-IFN
IL-15
Ly294002
E
Log2 fold increase (ChIPed DNA / input)
Mcm2 Mcm3 Mcm7 Dtl Kif11 Check1 Cdc25a
F
Phospho-E2F
Total E2F
MFI (Fold increase MCMV/NI)
Control α-CD122

Figure 6

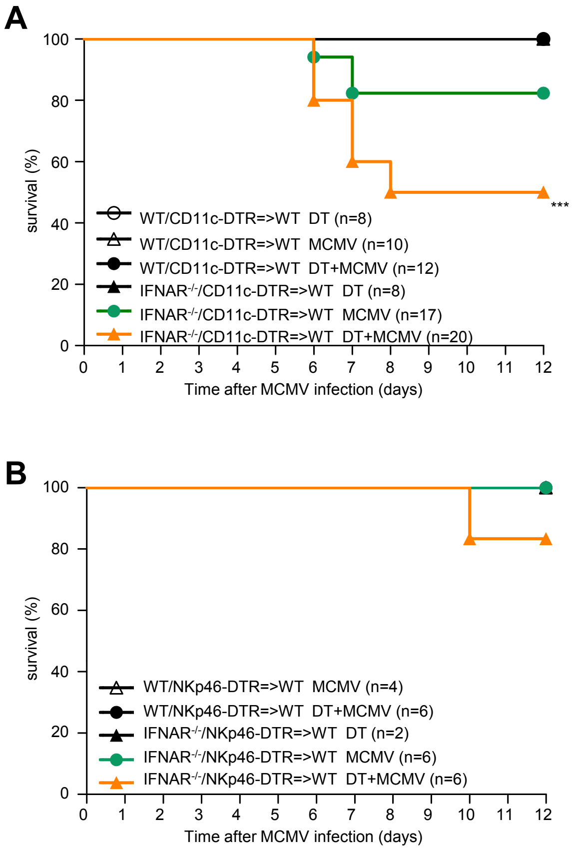
A
100
80
60
40
20
0
survival (%)
WT/CD11c-DTR=>WT DT (n=8)
WT/CD11c-DTR=>WT MCMV (n=10)
WT/CD11c-DTR=>WT DT+MCMV (n=12)
IFNAR-/-/CD11c-DTR=>WT DT (n=8)
IFNAR-/-/CD11c-DTR=>WT MCMV (n=17)
IFNAR-/-/CD11c-DTR=>WT DT+MCMV (n=20)
***
0 1 2 3 4 5 6 7 8 9 10 11 12
Time after MCMV infection (days)
B
100
80
60
40
20
0
survival (%)
WT/NKp46-DTR=>WT MCMV (n=4)
WT/NKp46-DTR=>WT DT+MCMV (n=6)
IFNAR-/-/NKp46-DTR=>WT DT (n=2)
IFNAR-/-/NKp46-DTR=>WT MCMV (n=6)
IFNAR-/-/NKp46-DTR=>WT DT+MCMV (n=6)
0 1 2 3 4 5 6 7 8 9 10 11 12
Time after MCMV infection (days)

Figure 7

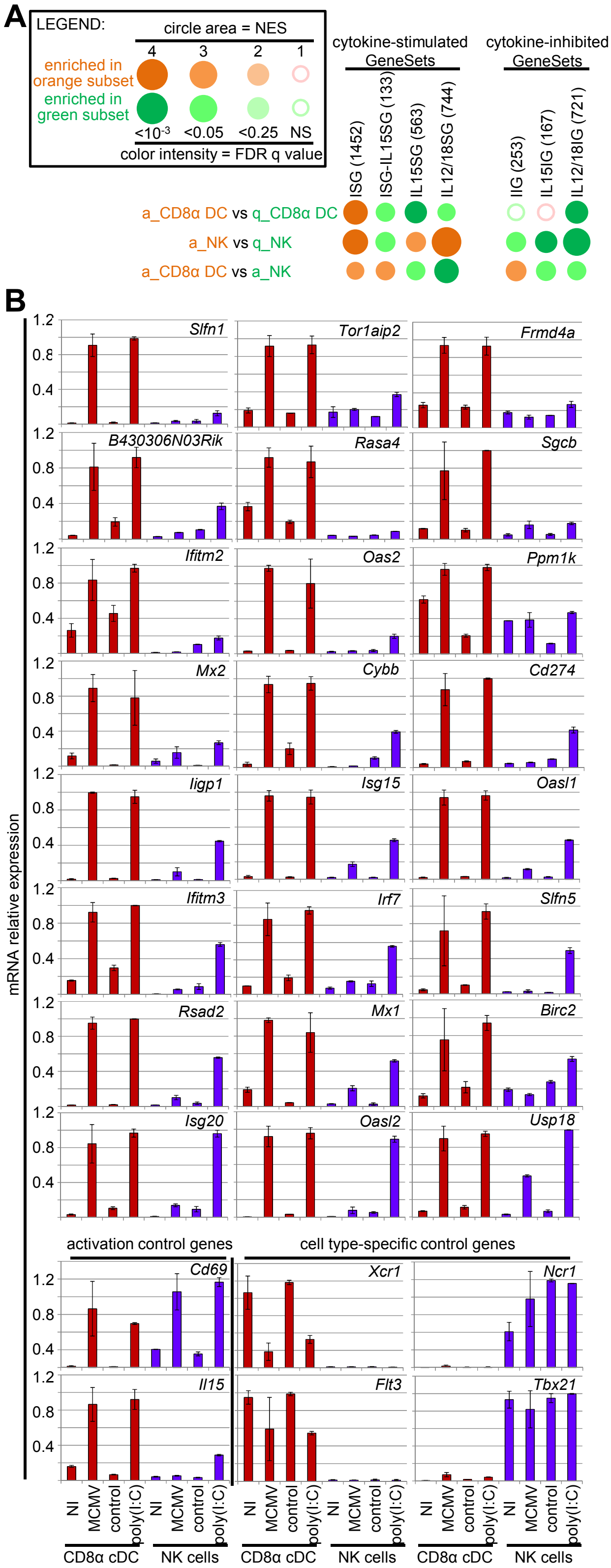

Supplemental Figure 1. Comparison of ISG induction in CD8α cDC and NK cells in vivo upon polyIC injection versus MCMV infection. Related to Figure 2. (A) GSEA of cytokine responding genes in CD8α cDC and NK cells isolated from the spleen of mice 3 hours after i.p. injection of 100 µg of polyIC. **(B)** Expression profiles of selected ISG and of cell-type specific control genes in CD8α cDC and NK cells isolated from the spleen of mice 3 hours after polyIC injection or 1.5 days after MCMV infection. Data are represented as arbitrary relative expression levels normalized to maximal expression across the different cell types (Y-axis). Data are shown as mean±SD for independent duplicates.

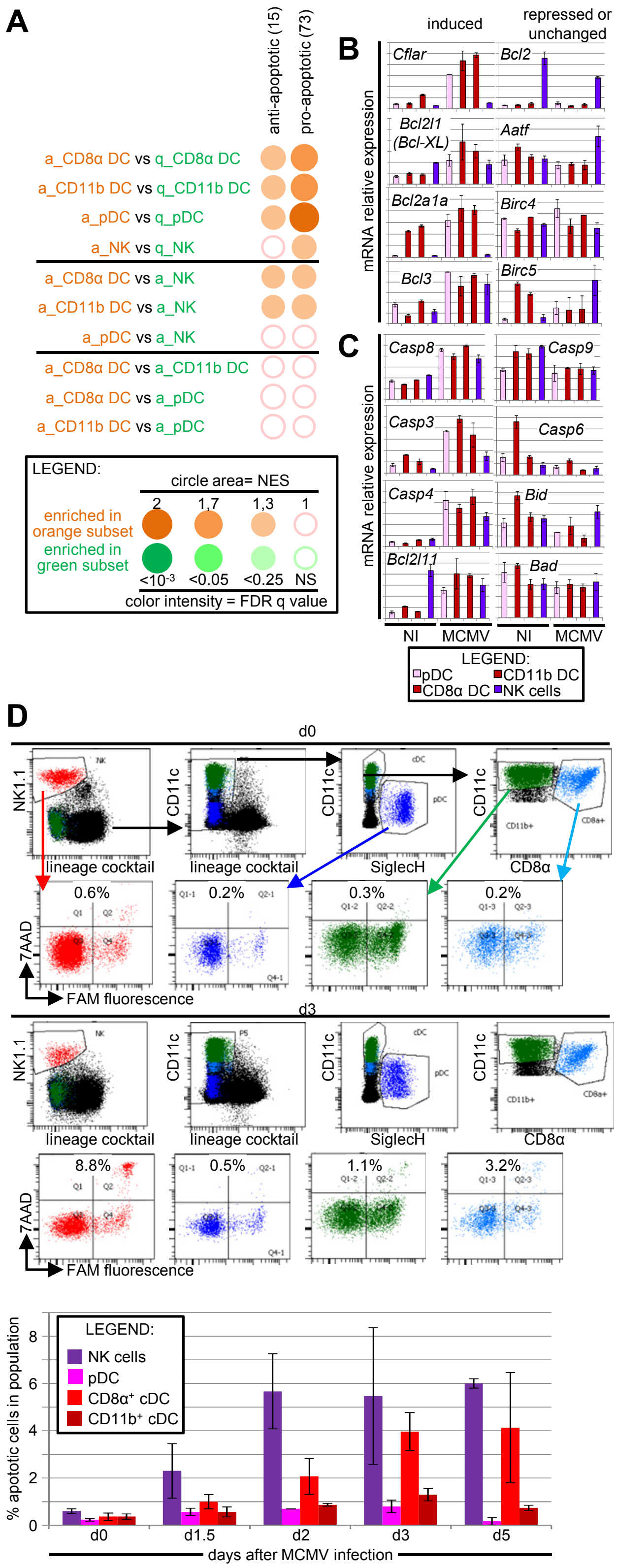

Supplemental Figure 2. Impact of MCMV infection on the apoptosis on DC subsets and NK cells. Related to Figure 3. (A) GSEA for anti-apoptotic and pro-apoptotic genes in DC subsets and NK cells isolated from the spleen of d1.5 MCMV-infected mice. **(B-C)** Expression profiles of selected anti-apoptotic **(B)** and pro-apoptotic **(C)** genes in DC subsets and NK cells isolated from the spleen of d1.5 MCMV-infected mice. Data are represented as arbitrary relative expression levels normalized to maximal expression across the different cell types (Y-axis). Data are shown as mean±SD for independent duplicates. **(D)** Frequency of apoptotic cells in DC subsets and NK cells isolated from the spleen of mice at different time points after MCMV infection. Within each leukocyte population, apoptotic cells are identified as double positive for caspase activity (FAM fluorescence) and plasma membrane permeability (7AAD staining). The lower graph shows results from one representative experiment out of 2. Data are shown as mean±SD, with at least 3 mice per group.

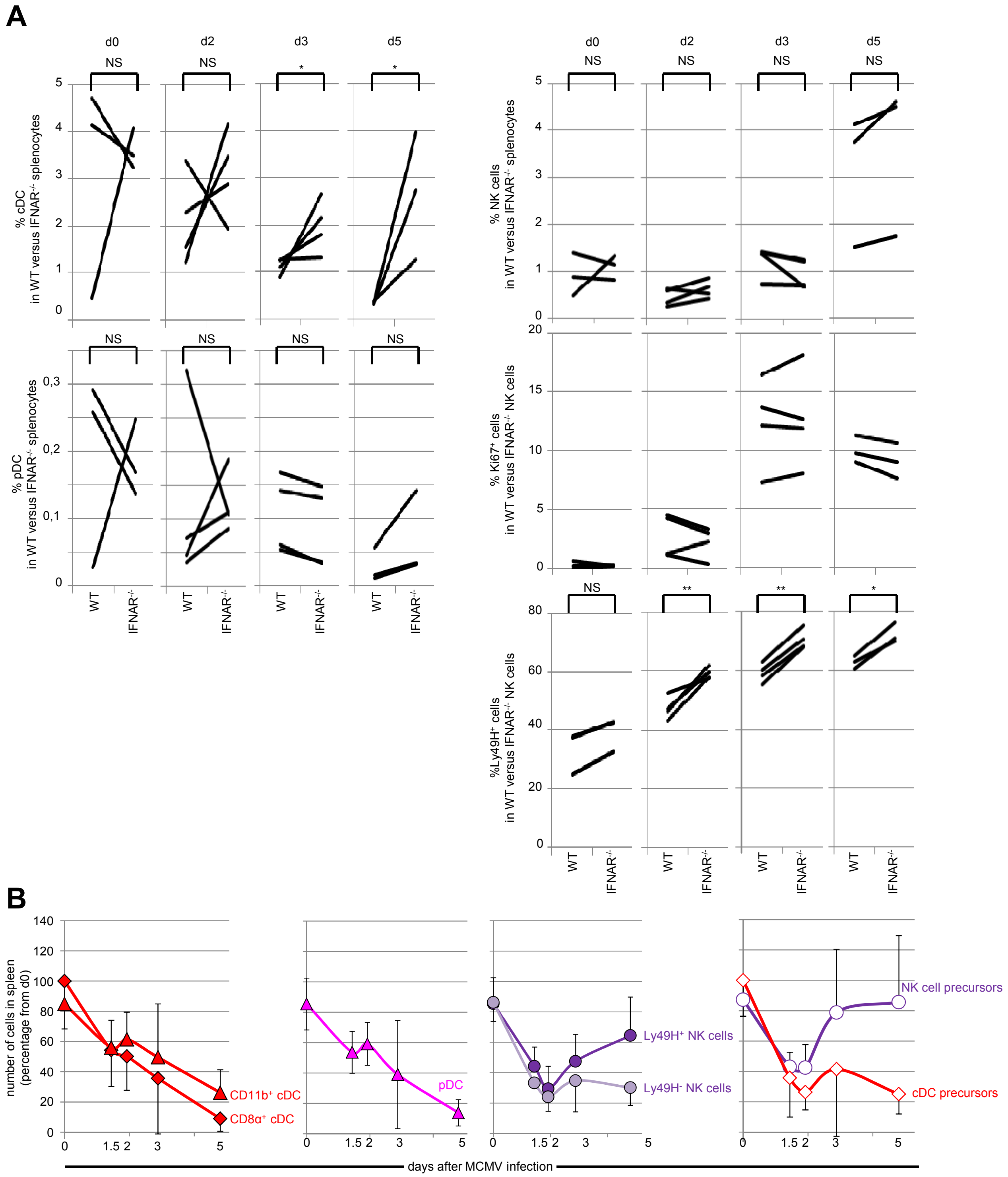

Supplemental Figure 3. MCMV infection interferes with cDC renewal through cell-intrinsic type I IFN effects likely acting in cDC immediate progenitors. Related to Figure 4. (A) Impact of cell-intrinsic responses to type I IFN on the dynamics of DC subset and NK cell numbers during MCMV infection. CD45.2-IFNAR$^{-/-}$/CD45.1-WT→CD45.1-WT BMC mice were infected or not with MCMV. Splenocytes were isolated at different time points after infection and the proportion of WT versus IFNAR$^{-/-}$ cells was measured within DC subsets and NK cells. The proportion of proliferating (Ki67^{+}) or of Ly49H^{+} cells was also examined in WT versus IFNAR$^{-/-}$ NK cells. Results are presented for each individual BMC mouse as a line linking the proportions of WT versus IFNAR$^{-/-}$ cells. Statistical analyses were performed using a paired two-tailed Student's t-test. **(B)** Impact of MCMV infection on the recruitment of DC or NK cell immediate progenitors in the spleen. WT C57BL/6 mice were infected with MCMV. Splenocytes were isolated at different time points after infection and the proportion of DC subsets, NK cells and their immediate progenitors were measured by flow cytometry. The data are shown as absolute numbers of cells in the spleen as a percentage from the levels measured before infection (mean±SD). The results are from one representative experiment of 2, with at least 3 mice per time point.

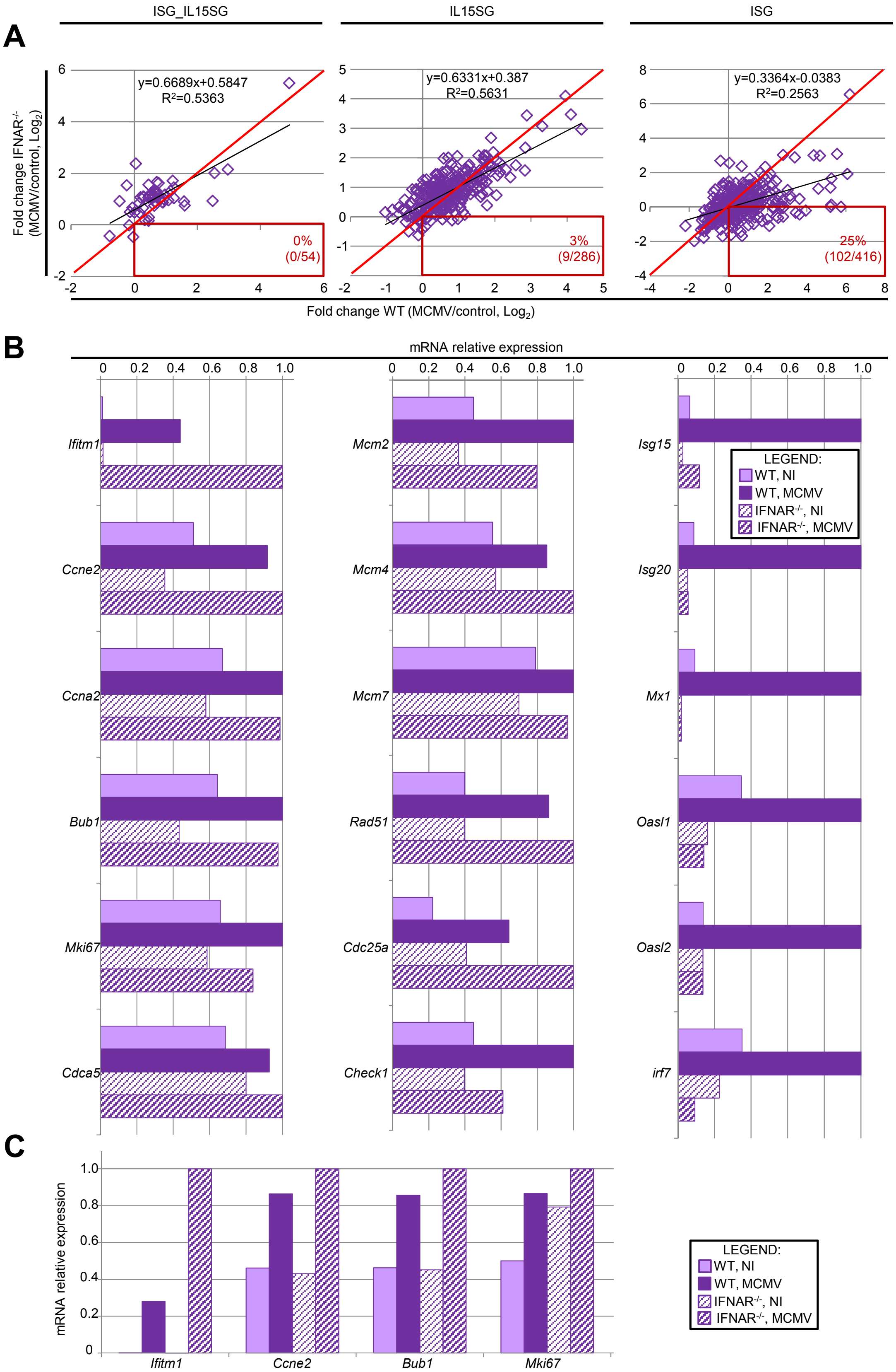

Supplemental Figure 4. ISG-IL15SG induction in NK cells infected mice does not require cell-intrinsic type I IFN responses. Related to Figure 5. (A) Genome wide analysis of the role of cell-intrinsic NK cell responses to type I IFN for the induction of ISG_IL15SG, IL15SG and ISG in d1.5 MCMV infected IFNAR$^{-/-}$/WT BMC mice. Data were generated as described in Supplemental Figure 3. **(A)** For each of the 3 GeneSets analyzed, for each individual gene, the fold change in IFNAR$^{-/-}$ NK cells (Y-axis) is plotted against the fold change in WT NK cells (X-axis). A linear regression curve is drawn and compared to the first diagonal. The percentage and numbers of the genes induced in WT NK cells but not changed or repressed in IFNAR$^{-/-}$ cells is shown in the red boxes. **(B)** Expression profiles of selected genes (Y-axis) from each GeneSet. Data are represented as arbitrary relative expression levels normalized to maximal expression across the different conditions (X-axis). **(C)** qRT-PCR confirmation of the expression profile of selected genes.

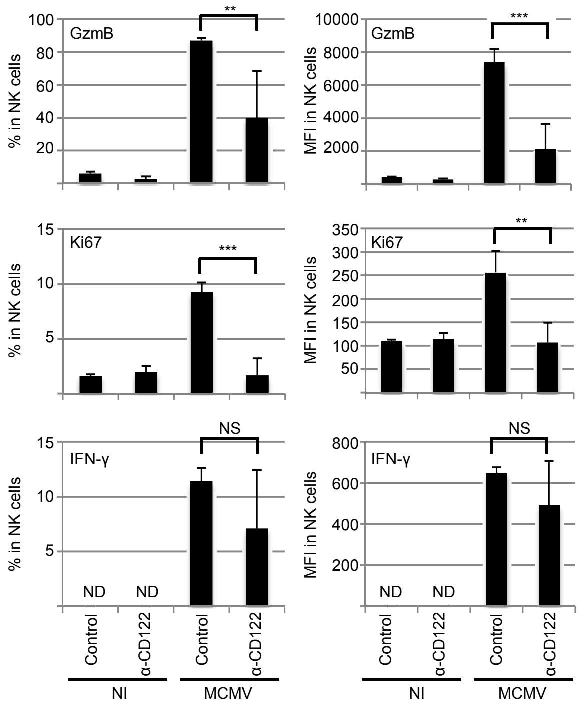

Supplemental Figure 5. Impact of *in vivo* neutralization of IL-15 responses on the expression of Granzyme B, Ki67 and IFN-γ in NK cells from MCMV-infected mice. Related to Figure 6. WT B6 mice were treated with $F(ab')_2$ anti-CD122 or control antibody and infected with MCMV. Spleens were harvested at 1.5 days after infection and the levels of GzmB, Ki67 and IFN-γ were measured in NK cells by flow cytometry. Results (mean±SD) are from one experiment representative of 2 with at least 4 animals per infected group. ND: not detectable.

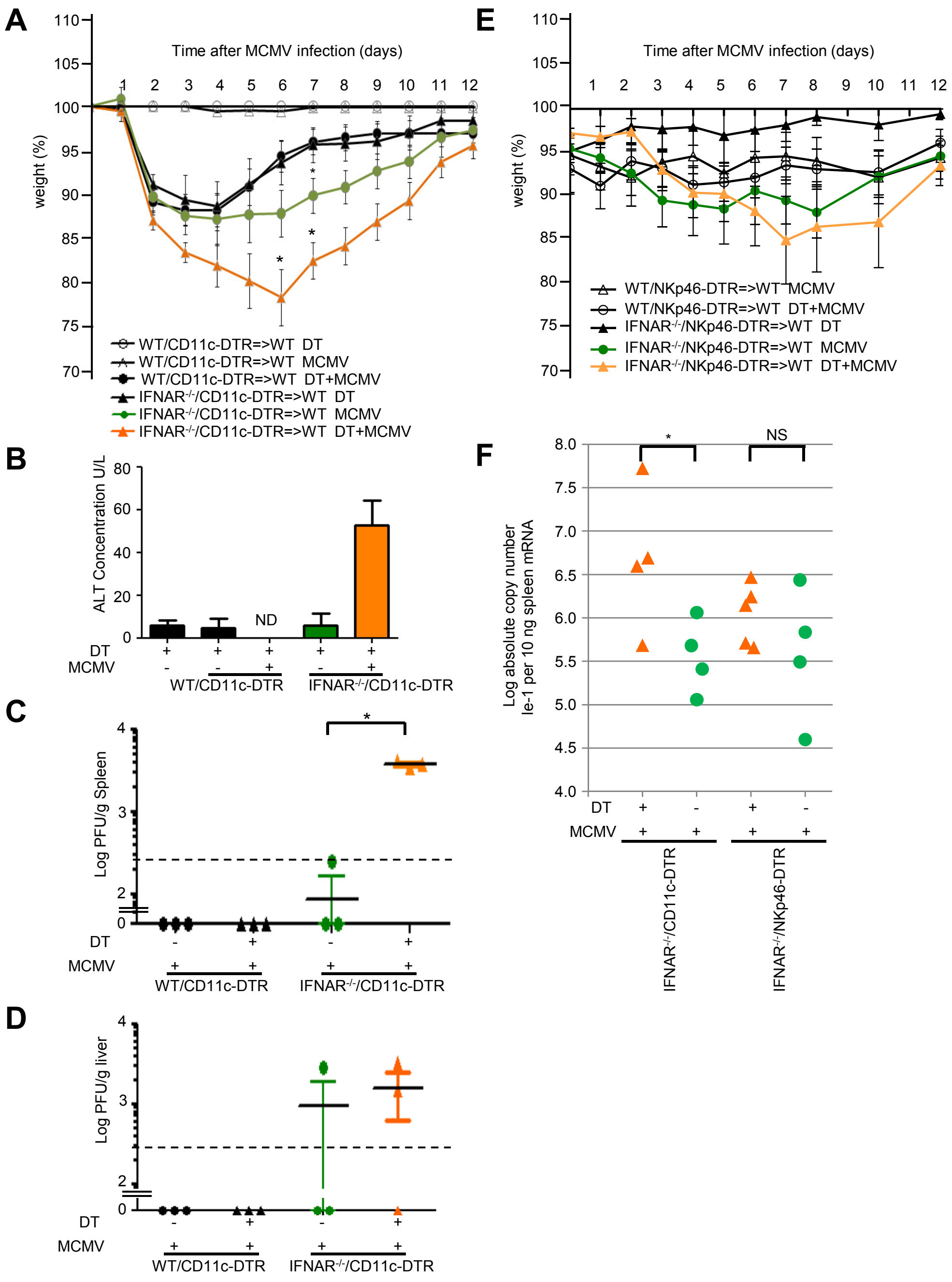

Supplemental Figure 6. DC but not NK cell ability to respond to type I IFN contributes to promote resistance to MCMV infection. Related to Figure 7. IFNAR$^{-/-}$/CD11c-DTR→WT and WT/CD11c-DTR→WT mixed BMC mice or IFNAR$^{-/-}$/NKp46-DTR→WT and WT/NKp46-DTR→WT mixed BMC mice were treated or not with 100ng of DT 24h before and 24h after infection with 10^4 pfu of MCMV. **(A, E)** Wasting (mean±SEM) is shown for 3 independent experiments pooled together for A and one experiment for E, for the same mice than survival in Figure 6. **(B-D, F)** Three days after MCMV infection, serum, spleen and liver were harvested for measurement of serum ALT levels **(B)** and viral titers **(C-D, F)**. Results are represented as mean±SEM (A-E), with 3 to 5 animals per group. (*=p<0.05).

Supplemental Table 1, related to Figure 1: see the hyperlink provided for the Excel spreadsheets

Supplemental Table 2, related to Figure 2: see the hyperlink provided for the Excel spreadsheets

Supplemental Table 3, related to Figure 3. Transcription factor binding site enrichment in cytokine-regulated genes modulated in DC or NK cells *in vivo* during MCMV infection

GeneSet[1]	matrix	Transcription factor	p-value
ISG	IRF7_01	Irf-7	$<10^{-6}$
	ISRE_01	ISGF3	$<10^{-6}$
	IRF_Q6 / IRF_Q6_01	Irf-1; Irf-10	$<2x10^{-4}$
	ICSBP_Q6	Irf-8	3.38x10-[4]
	TBX5_01	Tbx5	$3.95x10^{-4}$
	NFKAPPAB50_01	NF-kappaB (p50)	$4.90x10^{-4}$
	MIF1_01	MIF-1	$6.86x10^{-4}$
	STAF_01	Staf	$9.64x10^{-4}$
IL15 SG	E2F4DP1_01 / E2F_Q4_01 / E2F_03 / E2F_Q4 / E2F_Q6	Dp-1; E2f-1; E2F	10^{-6}
	PAX_Q6	Pax-1; Pax-2	10^{-6}
	CRX_Q4	Crx; Rx	$3x10^{-6}$
	E2F1_Q4_01 / E2F_Q6_01 / E2F1DP1RB_01 / E2F_02 / E2F_Q3 / E2F_Q3_01 / E2F1_Q6_01	Dp-1; E2f-1	$<1.65x10^{-4}$
	HNF3_Q6_01	Hnf-3; Hnf-3alpha	$3.54x10^{-4}$
	PITX2_Q2	Pitx2	$5x10^{-4}$
	E2F1_Q6	E2f-1	$5x10^{-4}$
	PAX6_Q2	Pax-6	$8.11x10^{-4}$
IL12/IL18 SG	ND[2]	N/A[3]	N/A
ISG/IL15SG	PAX6_Q2	Pax-6	$5x10^{-6}$
	CIZ_01	Ciz6-1; Ciz8	$4.5x10^{-5}$
	E2F_Q6_01 / E2F_Q4_01	Dp-1; E2f-1	$<1.54x10^{-4}$
	FOX_Q2	Foxd3; Foxf1	$5.54x10^{-4}$
	E2F_03	E2f-1	$6.26x10^{-4}$

[1]TFBS search was restricted to the genes from these GeneSets that were induced at least 2-fold in DC for ISG or in NK cells for IL-15-SG, IL12/18-SG and ISG/IL15-SG. [2]ND=none detected, i.e. no enrichment for any known TFBS. [3]N/A: not applicable

Supplemental Table 4, related to Figure 6: Primer sequences used for the qPCR analysis of ChIP-ed and input DNA samples

gene	sense primer	antisense primer	amplicon size (bp)	amplified region*
control	AAGGGGCCTCTGCTTAAAAA	AGAGCTCCATGGCAGGTAGA	140	chr8:76555801-76555940
Mcm2	GATCAGCCCATTCCTCACC	CGGGTCACGTGGTCTAGTTT	90	chr6:88864268-88864357
Mcm3	GCTCCACATCATCCAGCAC	GCGGGAAAACTTGGGAAG	119	chr1:20805326-20805444
Mcm7	TCCAGTGGACGCGGGAAT	GGTAGAGACCGGGTGACTTG	111	chr5:138401151-138401261
Dtl	AGGGATCGCTAAGGTTCTG	CCTGGCTGCTTACGTCAAT	123	chr1:193276020-193276142
Kif11	GCGTGCCGCTCTGCTATT	CAGGACGAACCTCCTCCTCT	100	chr19:37441466-37441565
Check1	CACACCTCTGCCGTAAAGC	GGCCACATCAGAATTTCAGC	126	chr9:36476321-36476446
Cdc25a	TAACGCTAAGGCCACTTTGG	TCCGACTAACTCGCCTCACT	102	chr9:109732973-109733074

*based on mouse genome mm8 (NCBI Build 36)

Supplemental Experimental Procedures

Flow cytometry

CMH-I (clone KH95), Ly6A (1A8), Ly6C (AL-21), CD86 (GL-1), CD40 (3/23), IFN-γ (XMG1), Ki67 (B56), Stat1 (1/Stat1), phospho-Stat1 (4a), Stat4 (8/Stat4) and phospho-Stat4 (38/p-Stat4) antibodies were purchased from BD biosciences. CCR7 (4B12), PDL1 (MIH5), OX40 (OX-86) and Fas-L (MFL3) were purchased from ebiosciences. GranzymeB (GB11) was purchased from Caltag. E2F1 (ab55398) and phopho-E2F1 (ab55325) were purchased from abcam. DC precursors were identified as viable, SiglecH$^-$, B220$^-$, CD19$^-$, CD3ε$^-$, NK1.1$^-$, CD11c$^+$, CMH-II$^-$, Sirpa^{int}, FLT3$^+$ cells (Liu et al., 2009). NK cell precursors were identified as viable, CD19$^-$, CD3ε$^-$, NKp46$^+$, CD27$^+$, CD11b$^-$ (Chiossone et al., 2009). Cell apoptosis was analyzed using the Vybrant FAM Poly caspases Assay kit (Invitrogen), following the recommendations from the supplier adapted for co-staining with 7AAD.

Cell sorting and mRNA preparation

Each cell type studied was sorted to over 98% purity (not shown) by flow cytometry using a FACSAria (BD Bioscience). Duplicate or triplicate samples were generated from independent experiments using pooled spleens of untreated, MCMV-infected or poly(I:C)-injected mice. Total RNA was prepared with RNeasy Isolation kits (QIAGEN). The quantity and integrity of mRNA were measured using the 2100 Bioanalyzer system (Agilent Technologies, France). The RNA integrity numbers were generally above 8 and never below 7.

Microarray data processing

Microarray experiments were performed as published (Robbins et al., 2008). Mouse 430.2 Affymetrix DAT files were processed using Affymetrix Gene Chip Operating System (GCOS) to generate .CEL files. Quality control of the array hybridization was performed through Bioconductor in the R statistical environment (version 2.10.1) using the affyPLM, Ringo and Amarge packages. This consisted in visual examination of raw hybridization chip images, boxplots of raw expression data, scatter plots and calculation of the Pearson's correlation coefficients between arrays, RLE and NUSE plots. Normalization of the raw Affymetrix expression data was performed by Robust Multi-chip Analysis (RMA) (Irizarry et al., 2003) using the affy package. Density plots of the normalized expression data were generated. Probesets not reaching a normalized expression value higher than 5 (log2 scale) across all arrays were considered as not expressed, and therefore were removed from the analysis. To select regulated probes between conditions, we used VAMPIRE (http://sasquatch.ucsd.edu/vampire/), a website implementing a statistical approach based on a modeling procedure that decomposes the variance structure of a microarray experiment into an expression-dependent and an expression-independent component (Hsiao et al., 2005; Subramaniam and Hsiao, 2012). This allowed us to extract significantly (FDR<=0.05) regulated probes in the comparison of conditions represented by duplicates, to which we subsequently applied a minimal fold change cut-off of 2, using a stringent 'min/max' procedure calculating fold change as (minimum expression among all replicates for all conditions selected/maximum expression among all other replicates for all other conditions) as previously published (Robbins et al., 2008).

Principal component analysis

Principal component analysis was performed using MeV (MultiExperiment Viewer version 10.2), considering all probesets of the microarrays, and represented under R and Bioconductor using the scatterplot3d package. Samples were clustered in a median center way.

GeneSet generation

The Ccnb2, Slfn1 and Cdkn2b GeneSets (Table S1) were generated by retrieving the 300 genes harboring the expression profile the most strongly correlated to that of the input gene, among all the expression profiles obtained from the mining of mouse 430 2.0 gene chips data present in the GEO database, using the COXPRESdb website (http://coxpresdb.jp/) (Obayashi and Kinoshita, 2011). Various sets of public expression data were used (Table S2) to identify genes which expression was modulated by innate cytokines under different experimental settings, based on statistical significance as assessed using the VAMPIRE microarray suite and on a 'min/max' fold change above 2. The different gene lists were then compiled together using Venn Diagram to generate GeneSets corresponding to genes stimulated or inhibited by unique or multiple cytokines (Table S2). The anti-apoptotic and pro-apoptotic GeneSets (Table S2) were generated based on literature (Reed et al., 2003; Youle and Strasser, 2008) and Mouse Genome Informatics (http://www.informatics.jax.org/) mining.

GSEA

GSEA tests the relative position of a collection of genes (GeneSet) within an independent, ranked data set (GeneList). Because GSEA relies on an additive signal of multiple genes within a data set, it is less dependent on arbitrary cutoffs, such as fold change of gene expression values, making its ability to detect an underlying process within transcriptomic data potentially more sensitive than a “single-gene” approach using traditional statistics. The use of rank data rather than absolute intensity measurements in GSEA also affords greater flexibility to make comparisons between diverse gene-expression data (i.e., between cell types, species, or array platforms) (Crozat et al., 2010). The statistical analysis was performed by evaluation of nominal p-value and false discovery rate (q-value) based on 1,000 random permutations between all the GeneSets identified here and with the GeneSets from cluster 2 of the Molecular Signatures Database (MSigDB) (Liberzon et al., 2011). Results were considered significant when the p-value was below 0.05 and when the q-value was below 0.25 (false discovery rate below 25%) accordingly to the recommendation from the software developers. In GSEA, genes were considered expressed differentially in a significant manner between conditions when they fall into the leading-edge (Subramanian et al., 2007).

Promoter sequence analysis for motif discovery

Promoter sequences of each gene were extracted using the Ensembl-retrieve-seq tool from RSAT (Turatsinze et al., 2008) which permitted to extract the 10000 nt upstream and 100 nt downstream of the TSS. When several TSS were identified for a gene, sequences were gathered in order to generate a unique record. Promoter sequences were truncated when a neighboring gene was found before reaching 10000 nt. RepeatMasker (http://www.repeatmasker.org) was used to withdraw the known mouse genome repeats and low complexity DNA sequences. These sequences were used to perform the *de novo* motif discovery approach with MEME (version 4.6.0) (Bailey and Elkan, 1994) and enriched oligonucleotides were compared to JASPAR, TRANSFAC and UNIPROBE databases using Tomtom (version 4.6.1) (Gupta et al., 2007).

ChIP_PCR experiments

Whole splenocytes were isolated by mechanical disruption from 25 C57BL/6 female mice (8-12 weeks old). Spleens were treated as pools of 3. After red blood cell lysis, cells were incubated with anti-mouse CD5, CD4, CD8α; anti-I-A/I-E and anti-Ly6C/G antibodies for 20 minutes on ice, washed twice with RPMI 10% FCS, resuspended with 600µl of prewashed Sheep anti-Rat IgG magnetic beads (Dynal, Invitrogen, France) diluted in 4 ml of RPMI 10% FCS, and incubated at 4°C for 30 minutes on wheel rotation. After two steps on magnetic stand, non-bound cells were harvested and incubated with FITC-conjugated anti-mouse CD4, CD8α, Ly6C/G and CD19 (BD Biosciences), PE-conjugated anti-NK1.1 (BD Biosciences), PerCP-eF710-conjugated anti-mouse NKp46 (eBiosciences, France). Dead cells were excluded by using Aqua Dead cell staining kit (Molecular Probes). Viable lineage^{-}NK1.1^{+}NKp46^{+} cells were sorted. An average of 10^{7} NK cells was harvested for each sorting, with over 98% purity. Cells were then stimulated 24 hours in RPMI 10% FCS supplemented with 2mM Glutammine, 10U/ml of Penicilin, 10µg/ml of Streptomycin, 50 µM of β-mercaptoethanol, 1 mM NaPyruvate, and 100 ng/ml of recombinant mouse IL-15 (Miltenyi, France). At the end of stimulation, the cells were washed and prepared for ChIP. 4 independent sorts were performed. Chromatin preparation for ChIP as well as qPCR validation experiments were performed as described previously (Koch et al., 2011), using ChIP-validated anti-E2F1 antibodies (clones KH20 and KH95, Millipore SAS, France) (Chen et al., 2008) and after optimization of the process to downscale it to 20 million cells cells as obtained by pooling the lysate of 2 sorts. This experiment was repeated twice independently. The genes and targeted sequences for the qPCR analysis of ChIP-ed and input DNA samples were selected upon the following criteria: i) belonging of the genes to the IL15SG geneSet, ii) implication of these genes in the promotion of cell proliferation, iii) induction of these genes in NK cells from MCMV-infected mice to the same levels in WT and IFNAR$^{-/-}$ cells, iv) detection of a putative E2F1 TFBS in promoter sequences based on our *in silico* analyses, and v) confirmation of E2F-binding to these putative TFBS in proliferating embryonic stem cells by analysis of published ChIP-seq raw data (Chen et al., 2008). Primers for the qPCR were designed on mouse genome mm8 (NCBI Build 36), using OligoPerfect™ Designer (Invitrogen). Specificity of the amplicons was tested using In silico PCR from the UCSC website. We also verified that the primers would not generate hairpins or dimers using OligoAnalyzer from IDT (Integrated DNA technologies). The primers are described in supplementary Table 3.

Titration of viral loads

Five days after MCMV infection, organs were harvested and mechanically disrupted in 1 ml of complete DMEM culture medium on ice. Viral loads were measured by conventional plaque assay on organ homogenates using NIH-3T3 cells (Pien et al., 2000) or by qRT-PCR on mRNA extracted from frozen tissues (Delale et al., 2005) with absolute quantification of ie-1 mRNA copy numbers using a standard curve for calculation (Wheat et al., 2003).

Supplemental References

Bailey, T.L., and Elkan, C. (1994). Fitting a mixture model by expectation maximization to discover motifs in biopolymers. Proc Int Conf Intell Syst Mol Biol *2*, 28-36.

Chen, X., Xu, H., Yuan, P., Fang, F., Huss, M., Vega, V.B., Wong, E., Orlov, Y.L., Zhang, W., Jiang, J.*, et al.* (2008). Integration of external signaling pathways with the core transcriptional network in embryonic stem cells. Cell *133*, 1106-1117.

Chiossone, L., Chaix, J., Fuseri, N., Roth, C., Vivier, E., and Walzer, T. (2009). Maturation of mouse NK cells is a 4-stage developmental program. Blood *113*, 5488-5496.

Crozat, K., Guiton, R., Guilliams, M., Henri, S., Baranek, T., Schwartz-Cornil, I., Malissen, B., and Dalod, M. (2010). Comparative genomics as a tool to reveal functional equivalences between human and mouse dendritic cell subsets. Immunol Rev *234*, 177-198.

Delale, T., Paquin, A., Asselin-Paturel, C., Dalod, M., Brizard, G., Bates, E.E., Kastner, P., Chan, S., Akira, S., Vicari, A.*, et al.* (2005). MyD88-dependent and -independent murine cytomegalovirus sensing for IFN-alpha release and initiation of immune responses in vivo. J Immunol *175*, 6723-6732.

Gupta, S., Stamatoyannopoulos, J.A., Bailey, T.L., and Noble, W.S. (2007). Quantifying similarity between motifs. Genome Biol *8*, R24.

Hsiao, A., Ideker, T., Olefsky, J.M., and Subramaniam, S. (2005). VAMPIRE microarray suite: a web-based platform for the interpretation of gene expression data. Nucleic Acids Res *33*, W627-632.

Irizarry, R.A., Hobbs, B., Collin, F., Beazer-Barclay, Y.D., Antonellis, K.J., Scherf, U., and Speed, T.P. (2003). Exploration, normalization, and summaries of high density oligonucleotide array probe level data. Biostatistics *4*, 249-264.

Koch, F., Fenouil, R., Gut, M., Cauchy, P., Albert, T.K., Zacarias-Cabeza, J., Spicuglia, S., de la Chapelle, A.L., Heidemann, M., Hintermair, C.*, et al.* (2011). Transcription initiation platforms and GTF recruitment at tissue-specific enhancers and promoters. Nat Struct Mol Biol *18*, 956-963.

Liberzon, A., Subramanian, A., Pinchback, R., Thorvaldsdottir, H., Tamayo, P., and Mesirov, J.P. (2011). Molecular Signatures Database (MSigDB) 3.0. Bioinformatics *27*, 1739-1740.

Liu, K., Victora, G.D., Schwickert, T.A., Guermonprez, P., Meredith, M.M., Yao, K., Chu, F.F., Randolph, G.J., Rudensky, A.Y., and Nussenzweig, M. (2009). In vivo analysis of dendritic cell development and homeostasis. Science *324*, 392-397.

Obayashi, T., and Kinoshita, K. (2011). COXPRESdb: a database to compare gene coexpression in seven model animals. Nucleic Acids Res *39*, D1016-1022.

Pien, G.C., Satoskar, A.R., Takeda, K., Akira, S., and Biron, C.A. (2000). Cutting edge: selective IL-18 requirements for induction of compartmental IFN-gamma responses during viral infection. J Immunol *165*, 4787-4791.

Reed, J.C., Doctor, K., Rojas, A., Zapata, J.M., Stehlik, C., Fiorentino, L., Damiano, J., Roth, W., Matsuzawa, S., Newman, R.*, et al.* (2003). Comparative analysis of apoptosis and inflammation genes of mice and humans. Genome Res *13*, 1376-1388.

Robbins, S.H., Walzer, T., Dembele, D., Thibault, C., Defays, A., Bessou, G., Xu, H., Vivier, E., Sellars, M., Pierre, P.*, et al.* (2008). Novel insights into the relationships between dendritic cell subsets in human and mouse revealed by genome-wide expression profiling. Genome Biol *9*, R17.

Subramaniam, S., and Hsiao, G. (2012). Gene-expression measurement: variance-modeling considerations for robust data analysis. Nat Immunol *13*, 199-203.

Subramanian, A., Kuehn, H., Gould, J., Tamayo, P., and Mesirov, J.P. (2007). GSEA-P: a desktop application for Gene Set Enrichment Analysis. Bioinformatics *23*, 3251-3253.

Turatsinze, J.V., Thomas-Chollier, M., Defrance, M., and van Helden, J. (2008). Using RSAT to scan genome sequences for transcription factor binding sites and cis-regulatory modules. Nat Protoc 3, 1578-1588.

Wheat, R.L., Clark, P.Y., and Brown, M.G. (2003). Quantitative measurement of infectious murine cytomegalovirus genomes in real-time PCR. J Virol Methods *112*, 107-113.

Youle, R.J., and Strasser, A. (2008). The BCL-2 protein family: opposing activities that mediate cell death. Nat Rev Mol Cell Biol *9*, 47-59.